1 **The blast effector Pwl2 is a virulence factor that modifies the cellular localisation of**
2 **host protein HIPP43 to suppress immunity.**
3

Vincent Were[1], Xia Yan[1], Andrew J. Foster[1], Jan Sklenar[1], Thorsten Langner[5], Amber Gentle[1], Neha Sahu[1], Adam Bentham[1], Rafał Zdrzałek[2], Lauren Ryder[1], Davies Kaimenyi[1], Diana Gomez De La Cruz[1], Yohan Petit-Houdenot[3], Alice Bisola Eseola[1], Matthew Smoker[1], Mark Jave Bautista[1], Weibin Ma[1], Jiorgos Kourelis[6], Dan Maclean[1], Mark J. Banfield[2], Sophien Kamoun[1], Frank L.H. Menke[1], Matthew J. Moscou[1,4] and Nicholas J. Talbot[1] *

[1] The Sainsbury Laboratory, University of East Anglia, Norwich Research Park, Norwich, NR4 7UH, United Kingdom.

[2] Department of Biochemistry and Metabolism, John Innes Centre, Norwich Research Park, Norwich, NR4 7UH, United Kingdom.

[3] Université Paris-Saclay, INRAE, UR BIOGER, 91120, Palaiseau, France.

[4] USDA-ARS Cereal Disease Laboratory, University of Minnesota, 1551 Lindig Street, Saint Paul, Minnesota, 55108 USA.

[5] Max-Planck-Institute for Biology, 72076, Tübingen, Germany.

[6] Imperial College London, Department of Life Sciences – Faculty of Natural Sciences, London, SW7 2AZ, United Kingdom

[*]Corresponding author: Nicholas J. Talbot (Nick.Talbot@tsl.ac.uk)

4

Abstract

The rice blast fungus *Magnaporthe oryzae* secretes a battery of effector proteins to facilitate host infection. Among these effectors, Pwl2 was first identified as a host specificity determinant for infection of weeping lovegrass (*Eragrostis curvula*) and is also recognised by the barley Mla3 resistance gene. However, its biological activity is not known. Here we show that *PWL2* expression is regulated by the Pmk1 MAP kinase during cell-to-cell movement by *M. oryzae* at plasmodesmata (PD)-containing pit field sites. Consistent with its regulation, we provide evidence that Pwl2 binds to a barley heavy metal-binding isoprenylated protein HIPP43, which results in its displacement from plasmodesmata. Transgenic barley lines overexpressing either *PWL2* or HIPP43 exhibit attenuated immune responses and increased disease susceptibility. By contrast, a Pwl2^{SNDEYWY} mutant that does not interact with HIPP43, fails to alter the PD localisation of HIPP43. Targeted deletion of three copies of *PWL2* in *M. oryzae* results in a *Δpwl2* mutant showing gain-of-virulence to weeping lovegrass and barley Mla3 lines, but also a reduction in severity of blast disease on susceptible host plants. Taken together, our results provide evidence that Pwl2 is a virulence factor that acts by suppressing host immunity through perturbing the plasmodesmatal deployment of HIPP43.

Introduction

Plant pathogens secrete virulence proteins called effectors during infection to suppress plant immunity and facilitate infection (Jones and Dangl, 2006). Fungal pathogens, such as the devastating blast fungus *Magnaporthe oryzae*, utilise an extensive battery of more than 500 effectors (Wilson and Talbot, 2009; Yan *et al.*, 2023), but very few have been functionally characterised (Oliveira-Garcia *et al.*, 2023a). A subset of effectors are recognized by plant intracellular nucleotide-binding leucine rich repeat (NLR) immune receptors to activate disease resistance. In rice for example, the paired NLRs RGA5/RGA4, Pik-1/Pik-2, and Piks-1/Piks-2 confer resistance to *M. oryzae* strains that secrete AVR1-CO39/AVR-Pia, AVR-Pik or AVR-Mgk1 effectors, respectively (Ashikawa *et al.*, 2008; Kanzaki *et al.*, 2012; Cesari *et al.*, 2013; Ortiz *et al.*, 2017; Zhang *et al.*, 2018; Sugihara *et al.*, 2023). These effectors are members of the *Magnaporthe* Avrs and ToxB-like (MAX) family which are sequence-unrelated, structurally conserved (de Guillen *et al.*, 2015) and overrepresented among effectors recognised by rice NLRs (Cesari *et al.*, 2013; Maqbool *et al.*, 2015). Pwl2 is a MAX effector first identified as a host specificity determinant that controls pathogenicity towards weeping lovegrass (*Eragrostis curvula*), a widely-grown forage grass (Sweigard *et al.*, 1995), and was recently shown to be recognised in barley by the Mla3 immune receptor (Brabham *et al.*, 2023). While Pwl2 has been widely studied to understand effector secretion and delivery (Mosquera *et al.*, 2009; Zhang and Xu, 2014; Oliveira-Garcia *et al.*, 2023b), the biological function of Pwl2 is unknown.

Recent studies of MAX-effector perception by NLRs have implicated host small heavy metal-associated (sHMA) domain containing proteins as potential targets of some of these effectors, including Pwl2 (Zdrzałek *et al.*, 2024). Small HMAs are highly expanded across plant species with putative functions including heavy metal detoxification and potential metallochaperones, but in most cases their functions are not known (Dykema *et al.*, 1999; Suzuki *et al.*, 2002; Gao *et al.*, 2009). HMAs can be broadly classified into two families, heavy metal-associated plant proteins (HPPs), and heavy metal-associated isoprenylated plant proteins (HIPPs), which possess a C-terminal isoprenylation motif (CaaX, where ‘a’ represents an aliphatic residue and ‘X’ is any amino acid) important for membrane anchoring (Hála and Žárský, 2019). The rice sHMA protein Pi21, for example, is a blast disease susceptibility factor (Fukuoka *et al.*, 2009), which has led to deployment of loss-of-function alleles of *pi21*, as a recessive form of rice blast resistance (Fukuoka *et al.*, 2009; Mutiga *et al.*, 2021). Furthermore, differences in host sHMA protein repertoires are linked to host-specific, adaptive evolution of the APikL2 effector family

(Bentham *et al.*, 2021). Importantly, HMA protein domains have been identified as non-canonical immune sensory domains in some NLR proteins, such as the rice Pik-1 of the Pik-1/2 and RGA5 of the RGA5/4 pair receptors respectively, essential for recognition of cognate *M. oryzae* effectors (Ashikawa *et al.*, 2008; Kanzaki *et al.*, 2012; Cesari *et al.*, 2013; Maqbool *et al.*, 2015). However, the function of sHMAs and their link to disease susceptibility is not understood, limiting our understanding of the role of MAX effectors in plant disease.

In this study we set out to investigate the biological function of *PWL2*. We were motivated to understand how a broadly distributed effector such as Pwl2 functions during a susceptible interaction between *M. oryzae* and its host. We report that *PWL2* has undergone extensive duplication and expansion in copy number with many rice blast isolates possessing 3-5 copies, making its functional analysis challenging. Using CRISPR-Cas9 gene editing, however, we have generated a *Δpwl2* mutant confirming that Pwl2 is a host specificity determinant but also revealing a hitherto un-recognized virulence function. Furthermore, we demonstrate here that *PWL2* expression during infection is controlled by the Pmk1 MAP kinase, which regulates cell-to-cell movement by the fungus at plasmodesmata-containing pit fields (Sakulkoo et al., 2018). We reveal that Pwl2 targets the HIPP43 sHMA protein in barley, thereby displacing it from plasmodesmata and show that transgenic plants overexpressing either *PWL2* or HIPP43 have reduced immune responses and greater susceptibility to blast disease. Finally, we show that a Pwl2^{SNDEYWY} mutant unable to interact with HIPP43 fails to displace it from PDs and cannot complement the reduced virulence of *Δpwl2* mutants. When considered together, our study provides evidence that Pwl2 is a virulence factor in *M. oryzae* that suppresses host defense by re-localising HIPP43 away from PDs to facilitate fungal invasion of plant tissue.

Results

Pwl2 is a cytoplasmic effector expressed during blast infection.

Expression of *PWL2* is specific to the initial biotrophic phase of plant infection, peaking at 48 hours post-infection (hpi) (Yan *et al.*, 2023) (**Fig. S1A - C**). The Pwl2 effector localises in the biotrophic interfacial complex (BIC), a plant membrane-rich structure –that is clearly visible as a single bright punctum, initially at the tip of a penetration hypha and then adjacent to bulbous, branched invasive hyphae (Khang *et al.*, 2010). The BIC is the predicted site of effector delivery (Kankanala *et al.*, 2007; Giraldo *et al.*, 2013; Oliveira-Garcia *et al.*, 2023b; Were and Talbot, 2023), although experiments to date have not precluded that the BIC could be a site of effector sequestration from the host plant. To investigate this possibility, we

95 generated a single *M. oryzae* strain expressing two BIC-localised effectors Pwl2-mRFP and
96 Bas1-GFP and visualised their localisation during infection of leaf sheath tissue in the
97 susceptible rice cultivar Moukoto. The two effectors were observed as small punctate signals
98 within the same BIC (**Fig. 1A and B**). By contrast, when two different *M. oryzae* strains,
99 Ina168 and Guy11, expressing Pwl2-GFP and Pwl2-mRFP respectively were used to
100 simultaneously infect rice tissue, we observed that the BIC formed by each individual invasive
101 hypha exclusively contained either Pwl2-GFP or Pwl2-mRFP respectively but never both
102 fluorescence signals (**Fig. 1C and D).** This is consistent with Pwl2 secretion by each fungal
103 strain into the BIC, because sequestration of previously secreted Pwl2 from the plant cytoplasm
104 to the BIC would result in a mixed GFP/mRFP fluorescence signal in the BIC. We conclude
105 that Pwl2 is expressed early during infection and secreted to the BIC from where it is delivered
106 into host cells.
107
108 ***PWL2* expression is regulated by the Pmk1 MAP kinase during invasive growth.**
109 The blast fungus invades rice tissue by means of pit field sites containing plasmodesmata
110 (PDs), which enable it to move between rice cells while maintaining integrity of the rice plasma
111 membrane. PD conductance is also regulated by the fungus, enabling effectors like Pwl2 to be
112 deployed in adjacent uninfected cells (Kankanala et al., 2007; Sakulkoo et al., 2018). Cell-to-
113 cell movement by the fungus is regulated by the pathogenicity mitogen-activated protein kinase
114 1 (Pmk1 MAPK) pathway. An analogue-sensitive mutant of Pmk1 has been shown to be unable
115 to move through pit fields in the presence of the MAPK inhibitor 1NA-PP1 (Sakulkoo et al.,
116 2018). Given that *PWL2* is expressed during the initial stages of infection, we decided to test
117 whether it is regulated by Pmk1. We therefore re-analyzed RNA-seq data (**Fig. 1E**) (Sakulkoo
118 *et al.*, 2018) by separating raw reads of *M. oryzae* and *O. sativa* and quantifying transcript
119 abundance using Kallisto, followed by determining differential expression using Sleuth. We
120 found that *PWL2* is significantly down-regulated in a *M. oryze pmk1*^{AS} mutant during cell-to-
121 cell movement in the presence of 1NA-PP1 together with a subset of known effector genes -
122 *BAS83*, *BAS52*, *BAS2, AVR-Pita-1, BAS3, BAS4, BAS162* and *AVR-Pik-C* (**Fig. 1F**). By
123 contrast, *MoNLP1* showed up-regulation, while expression of actin (MGG_03982) and the
124 RP27 40S 27a ribosomal subunit genes (MGG_02872) were not significantly affected (**Fig.
125 1F**). We then used live cell imaging to investigate Pwl2-GFP expression in a *pmk1*^{AS} mutant
126 during rice leaf sheath infection ±1Na-PP1. We initially observed Pwl2-GFP in the BIC at early
127 stages of infection, unaffected (Stage 1) 30-36hpi (**Fig. 1G and H**), as previously reported
128 (Sakulkoo *et al.*, 2018), but by later stages of infection Stage 2 (36-40hpi), (**Fig. 1I-J**), and

129 Stage 3 (40-48hpi) (**Fig. 1K-L**), 14-22h after 1NA-PP1 treatment, Pwl2-GFP fluorescence was
130 significantly reduced (**Fig. 1J, L and M**). The reduction in Pwl2-GFP fluorescence was
131 consistently associated with the stage at which *M. oryzae* traverses PD-containing pit field sites
132 and enters adjacent plant cells. Taken together, we conclude that Pwl2 is regulated by the
133 Pmk1 MAPK signalling pathway during cell-to-cell invasive growth by *M. oryzae.*

134 ***PWL2* is highly conserved in *M. oryzae.***

135 *PWL2* belongs to a large gene family (Kang *et al.*, 1995; Sweigard *et al.*, 1995), but its
136 conservation in the global rice blast population is not known. We therefore investigated *PWL*
137 gene family distribution in isolates that infect a variety of different grass species (**Fig. 2A**) This
138 revealed that *PWL2* is found in the majority of host-limited forms of *M. oryzae* and related
139 *Magnaporthe* species, except for *Setaria* and closely-related *Panicum, Cynodon* and *Urochloa*-
140 infecting isolates (although these were less well represented than other isolates) as shown in
141 **Fig. 2A**. By contrast, *PWL1* is present in a sub-set (Asuke *et al.*, 2020) of *Eleusine*-infecting
142 isolates and some *Oryza*-infecting isolates, but largely absent from other host-specific lineages,
143 except one *Eragrostis*-infecting isolate (EtK19-1), and one *Cynodon*-infecting isolate
144 (Cd88215) (**Fig. 2A)**. Similarly, *PWL3* is present in most *Oryza*-infecting isolates, some
145 *Setaria*, *Lolium*, and *Eleusine*-infecting isolates, but largely absent in *Eragrostis, Triticum*,
146 *Digitaria* and *Pennisetum* lineages, while *PWL4* is present in *Eleusine*, *Eragrostis, Lolium* and
147 *Triticum*-infecting isolates, *Pennisetum* and *Digitaria*-infecting isolates, but only two *Oryza*-
148 infecting isolates (**Fig. 2A)**. We conclude that the *PWL* gene family (Kang *et al.*, 1995) is
149 broadly distributed among blast fungus isolates infecting numerous grasses but that *PWL2*, is
150 widespread across rice-infecting isolates and the majority of host-limited forms of *M. oryzae.*
151

152 Having determined that *PWL2* is broadly distributed in *M. oryzae*, we next sought to determine
153 its allelic variability. In addition to a loss of recognition allele *pwl2-2*, which contains a single
154 Asp-90-Asn substitution (Sweigard *et al.*, 1995), we identified 14 new alleles of *PWL2* (**Fig.**
155 **S2A**). Notably, most polymorphic residues occur between positions His87 to Ser92, suggesting
156 these residues might contribute to Pwl2 recognition by a cognate resistance gene (**Fig. S2A**).
157 Interestingly, we could only identify 1 variant of *PWL1*, 5 variants of *PWL3* and 1 variant of
158 *PWL4*, despite these effector genes occurring in finger millet, rice, wheat and ryegrass-
159 infecting lineages, respectively (**Fig. 2A and S2B - S2D**). It is possible that sample size for
160 some host-specific lineages may lead to an underestimate of allelic variability in *PWL1, PWL3*,
161 and *PWL4,* but from this analysis *PWL2* appears to be highly polymorphic and conserved,

162 compared to other members of the gene family (**Fig. S2E**). We also tested the ability of a subset
163 of *PWL2* alleles to be recognised by barley *Mla3*. In some cases, we found variant *PWL2* alleles
164 occurred in a *M. oryzae* isolate carrying *PWL1* (such as U34 and E39) or isolates with multiple
165 copies of *PWL2* (for example TH3), precluding functional analysis, and not all isolates were
166 available for testing. As expected, Guy11 did not produce lesions on cv. Baronesse, but was
167 able to infect cv. Nigrate (**Fig. S3A – C**). However, JUM1 (*pwl2-2*), BTJP4-16 (*pwl2-3)* and
168 BN0293 (variant *pwl2*) all caused blast disease on cv. Baronesse, confirming that they contain
169 loss of recognition *pwl2* alleles (**Fig. S3A - C**). Pwl2 has recently been structurally described
170 as a MAX effector, containing a core β-sandwich fold formed of two antiparallel β-sheets, as
171 well as a single α-helix, C-terminal to the β-sandwich fold (Zdrzałek *et al.*, 2024). We were
172 interested to understand how these variable residues affect Pwl2 recognition. We therefore
173 mapped a subset of the identified variants of Pwl2 to the effector crystal structure. We noted
174 that all polymorphic residues in *pwl2* alleles, such as the Glu-89-Gln, Lys-91-Gln and Ser-92-
175 Ile substitutions in *pwl2-3,* were present in the C-terminal α-helix, a distinct region from the
176 core MAX-fold (**Fig. 2B**). We conclude that this interface is likely used by immune receptors
177 present in resistant barley (Mla3) and weeping lovegrass to bind Pwl2 and is potentially
178 stabilized by the MAX-fold.

179 ***PWL2* has undergone copy number expansion in *M. oryzae*.**

180 *PWL2* copy number appears to vary significantly among *M. oryzae* isolates. The *M. oryzae*
181 reference genome assembly (strain 70-15) has two copies of *PWL2* on chromosomes 3 and 6,
182 annotated as MGG_04301 and MGG_13683, respectively (Dean *et al.*, 2005). Southern blot
183 hybridization (**Fig. S4**), however, and analysis of long-read assembled genome sequence of *M.*
184 *oryzae* Guy11 identified three copies of *PWL2* (**Fig. 3A).** *PWL2* loci were associated with
185 *MGR583*, *POT2* and *MAGGY* transposable elements, suggesting their potential involvement in
186 genome rearrangements (**Fig. 3A)**. To further assess *PWL2* copy number variation in *M. oryzae*
187 isolates, we employed k-mer analysis to determine copy number variation of *PWL2* in 286 *M.*
188 *oryzae* genomes. Copy number variation is common among effector-encoding genes, such as
189 *AVR-Pik*, *AVR-Pizt, BAS1, BAS4* and *SLP1*, but was particularly prevalent for *PWL2* with one
190 isolate, for instance, containing 9 copies (**Fig. 3B).** We conclude that *PWL2* has expanded in
191 copy number in *M. oryzae*.

192 **Pwl2 is both a host range determinant and a virulence factor**
193 We next set out to determine the function of *PWL2* in blast disease through gene functional
194 analysis. Given that *PWL2* occurs in multiple copies, we used CRISPR/Cas9 genome editing
195 (Foster *et al.*, 2018) to simultaneously delete all three copies of *PWL2* found in Guy11. We
196 designed a sgRNA to target *PWL2* and introduced a hygromycin phosphotransferase (*HPH*)
197 encoding gene cassette (**Fig. 4A)**. Transformants with ectopic integrations, or where some
198 *PWL2* had not been deleted, gave a predicted PCR amplicon of 645 bp in size. By contrast,
199 *Δpwl2* mutants generated a larger amplicon of 1.5 kb (**Fig. 4A**). Four putative transformants
200 were selected for whole genome sequencing. Raw reads were aligned to the *M. oryzae*
201 reference genome using samtools v.15, before converting into BAM files and visualising using
202 IGV viewer. No reads mapping to the *PWL2* locus were identified in mutants T6 and T12,
203 whereas fewer reads mapped to the same locus from sequenced T4 and T5 (**Fig. S5A**). This
204 confirmed that T6 and T12 are *Δpwl2* transformants. Transformant T4, T5 and T6 displayed
205 vegetative growth that was identical to Guy11 with normal dark concentric rings and light
206 growing edges, while T12 showed slight reduced growth, melanisation and conidiation (**Fig.**
207 **S5B)**. Given that *PWL2* is a host range determinant and avirulence gene, we reasoned that *M.*
208 *oryzae Δpwl2* deletion mutants would gain virulence on weeping lovegrass (Kang *et al.*, 1995;
209 Sweigard *et al.*, 1995) and barley cv. Baronesse expressing *Mla3* (Brabham *et al.*, 2023). The
210 *Δpwl2* deletion transformants T5, T6 and T12 and Guy11 were therefore used to infect weeping
211 lovegrass seedlings and barley Baronesse using spray inoculation. The *Δpwl2* mutant T6
212 produced disease symptoms identical to those produced by *Eragrostis*-infecting isolate G17
213 and *Oryza*-infecting isolate Ina168 which lacks *PWL2,* while Guy11 and the two
214 complemented isogenic strains (T6+*PWL2*p:*PWL2*) and (T6+*RP27*p:*PWL2*) were unable to
215 cause disease (**Fig. 4B**). Similarly, T5 and T12 also produced disease symptoms on weeping
216 lovegrass seedlings and cv. Baronesse (**Fig. S5C**). We conclude that T5, T6 and T12 are loss
217 of recognition mutants of *PWL2* (**Fig. 4B and S5C**), and we can be confident that T6 and T12
218 have complete deletion of all three copies of the gene.
219
220 We next tested whether Pwl2 has a virulence function during a compatible interaction between
221 the blast fungus and its host. Having observed that T12 had slight differences in vegetative
222 growth, we decided to select T6 for virulence assays and as a genetic complementation
223 background for *PWL2*. T6 was used to inoculate susceptible rice cultivar CO39 by spray
224 infection, and on susceptible barley lines cv. Nigrate (-*Mla3)*, Siri (+*Mla8*), cv. Golden Promise

225 (+*Mla8*), and resistant cv. Baronesse (+*Mla3*) using leaf drop inoculation. In four independent
226 replicates, the *Δpwl2* mutant T6 showed a reproducible reduction in virulence on CO39
227 compared to wildtype Guy11 or a complemented isogenic strain (T6+*PWL2*p:*PWL2*), based
228 on lesion density and lesion length (**Fig. 4C - E)**. As expected, T6 was able to cause blast
229 disease on cv. Baronesse unlike Guy11 and produced statistically smaller lesion sizes on barley
230 lines Siri and Golden Promise, compared to Guy11. Both strains were able to infect Nigrate
231 (**Fig. 4F and G**). We conclude that *PWL2* contributes to the ability of *M. oryzae* to cause blast
232 disease.

233 **Pwl2 suppresses host immunity**

234 Having determined that the Pwl2 effector contributes to virulence, we decided to study its
235 biological function during host cell colonisation. To do this we first generated stable transgenic
236 barley lines (in cv. Golden Promise) expressing *PWL2-YFP* (without its signal peptide) under
237 control of the CaMV35S promoter (**Fig. 5A)**. We tested two independent *PWL2-YFP*
238 transgenic plants for their response to two elicitors of PAMP-triggered immunity (PTI), flg22
239 and chitin, compared to wild type cv. Golden Promise (**Fig. 5A)**. Barley perceives flg22
240 through the pattern recognition receptor FLS2 and chitin through HvCEBiP and HvCERK1,
241 leading to immune responses such as generation of reactive oxygen species (ROS) (Yu *et al.*,
242 2023). We observed that Pwl2 expression abolished flg22 (**Fig. 5B - C)** and chitin-induced
243 ROS generation (**Fig. 5D - E)**. Pwl2 therefore contributes to virulence by suppressing PTI
244 during compatible interactions. To investigate the effect of elevated Pwl2 effector expression
245 on blast infection, we infected two independent transgenic barley plants expressing *PWL2* with
246 *M. oryzae* Guy11. *PWL2*-expressing barley lines were more susceptible and developed blast
247 disease symptoms earlier (2-3 dpi) compared to infection of isogenic cv. Golden Promise (**Fig.
248 5F and G)**. We conclude that Pwl2 acts as a modulator of PTI that helps facilitate fungal
249 infection.

250 **Pwl2 interacts with the heavy metal binding isoprenylated protein HIPP43.**

251 To determine the likely target of Pwl2, transgenic barley lines expressing Pwl2-YFP were used
252 in co-immunoprecipitation coupled to mass spectrometry (IP-MS) analysis. This was followed
253 by spectral search in the *H. vulgare* (barley, cv Morex version 3) proteome database. We
254 identified a total of 282 frequently occurring proteins in the eight biological replicates
255 containing Pwl2, that were not identified in the six free-YFP control samples. To avoid
256 focusing on false positives in the form of sticky and abundant proteins, fold-changes were

257 calculated by first determining the average number of peptides per protein candidate, before
258 estimating $\log_2$ fold change compared to the control experiment. We further filtered for proteins
259 that produced at least two peptide hits in more than half of replicates (≥4/8 biological
260 replicates). A total of 52 proteins met this criterion and were considered as enriched in samples
261 compared to controls and were therefore selected for further analysis. Furthermore, because
262 Pwl2 attenuates the ROS-burst in barley transgenic lines, we focused initially on protein
263 candidates previously reported to have potential roles in immunity or ROS generation (**Fig.
264 6A)**. These were selected for one-to-one interactions using a yeast-two-hybrid (Y2H) assay by
265 co-transforming constructs expressing Pwl2 and Putative Pwl2 Interacting Proteins (PPIPs)
266 identified by IP-MS (**Fig. 6A)**. Pwl2 showed a strong interaction with PPIP4, a HMA-domain
267 protein (**Fig. 6B)**. We named this protein *Hv*HIPP43, for *Hordeum vulgare* heavy metal domain
268 containing isoprenylated plant protein 43 based on homology to *Os*HIPP43 (Zdrzałek *et al.*,
269 2024). We also tested to ensure that neither Pwl2 nor HIPP43 demonstrated auto-activity in
270 yeast-2-hybrid drop out media (**Fig. S6A**). To independently verify the interaction between
271 Pwl2 and HIPP43, we carried out co-immunoprecipitation (co-IP) analysis using protein
272 extracts from *N. benthamiana* and confirmed that *Hv*HIPP43 interacts with Pwl2-YFP (**Fig.
273 6C and D)**. Conversely, three other MAX-fold effectors, MEP3, AVR-PikE, AVR-Piz-t, or
274 free YFP did not interact with HIPP43 (**Fig. 6D)**. We next tested whether *PWL* gene family-
275 encoded proteins Pwl1, Pwl3, Pwl4 and the pwl2-3 variant could also interact with *Hv*HIPP43
276 and showed that they can all interact based on Y2H assays, suggesting that Pwl2 belongs to an
277 effector family that interacts with a host sHMA protein (**Fig. 6E)**. By contrast, three MAX-
278 fold effectors AVR-Pia, AVR-PikD and AVR-Mgk did not interact with HIPP43 (**Fig. 6E)**.
279 Barley and wheat have three copies of HIPP43 per haploid genome, but based on our IP-MS
280 results, we identified peptides that mapped to two copies of HIPP43, which both strongly
281 interacted with Pwl2 in Y2H assays HIPP43 (**Fig. S6B-C)**.

282 **Pwl2 can interact with HIPP43 orthologs of diverse grass species.**

283 HIPPs are expanded in plant genomes and to test whether HIPP43 has orthologs in other grass
284 species, we generated a maximum likelihood phylogenetic tree of HMA domains from diverse
285 grasses with high quality genomes and annotations (**Fig. S6D**). The HIPP43 family formed a
286 distinct clade which includes orthologs from rice (*O. sativa)*, wheat (*T. aestivum*)*,* wild wheat
287 (*Haynaldia villosa*), foxtail millet (*S. italica*)*,* weeping lovegrass (*E. curvula*)*,* Sorghum
288 (*Sorghum bicolor*), *Oropetium thomaeum*, *Zea mays* and *Brachypodium distachyon* (**Fig.
289 S6D**). Furthermore, we could identify copy number variation ranging from one to five copies

290 in grasses, with barley and wheat (i.e. *Triticeae* lineage) having three or more paralogs of
291 HIPP43, one per haploid genome (**Fig. S7A**). We found that Pwl2 interacts with *Hv*HIPP43
292 orthologs from rice (*Os*HIPP43), *Triticum* (*Taes*HIPP43), *Setaria* (*SitiHIPP43*), *Eragrostis*
293 (*Ec*HIPP43) and *Haynaldia* (HIPP1-V) in Y2H assays (**Fig. 6F)**. The interaction of Pwl2 with
294 rice *Os*HIPP43 was verified by *in vitro* biochemistry and a structure of the complex was
295 obtained by *X*-ray crystallography (Zdrzałek *et al.*, 2024). We also analyzed the transcriptional
296 profile of *Os*HIPP43 during infection of Guy11 in a susceptible rice line CO39 (Yan *et al.*,
297 2023) and found that *Os*HIPP43 expression is up-regulated during plant infection, consistent
298 with a role in host defense (**Fig. S7B)**.

299 **Overexpression of HIPP43 suppresses PTI and increases blast susceptibility.**
300 To investigate the role of the Pwl2-HIPP43 interaction, we generated barley transgenic lines
301 overexpressing *Hv*HIPP43. Two independent transgenic lines were challenged with two PTI
302 elicitors, flg22 (**Fig. 7A-B)** and chitin (**Fig. 7C-D)**. Strikingly, we observed that both the chitin
303 and flg22-induced ROS burst was abolished in plants expressing *Hv*HIPP43, compared to wild
304 type (**Fig. 7A-D)**. Similarly, when we challenged transgenic barley plants expressing
305 *Hv*HIPP43 with *M. oryzae*, we observed increased susceptibility compared to the wildtype cv.
306 Golden Promise, and disease lesions appeared earlier than in wild type plants (**Fig. 7E and F)**.
307 These findings are consistent with over-expression of both *PWL2* and HIPP43 leading to
308 enhanced blast disease susceptibility.

309 **Pwl2 prevents plasmodesmatal localisation of HIPP43.**
310 To investigate the function of *Hv*HIPP43, we performed live cell imaging following transient
311 expression in *N. benthamiana* to determine its sub-cellular localisation. When tagged at the N-
312 terminus (mCherry-HIPP43), *Hv*HIPP43 localised predominantly to puncta at the plasma
313 membrane that co-localise with callose staining (aniline blue), consistent with sites of
314 plasmodesmata (PD) (**Fig. 7G and H)**. Like all HIPPs, *Hv*HIPP43 has an isoprenylation motif
315 at its C-terminus (**Figure S8A and B**), implicated in membrane anchoring (Hála and Žárský,
316 2019), so we investigated whether PD localisation is affected by its deletion. We observed that
317 PD localisation was indeed abolished in the absence of the isoprenylation motif and -Iso-
318 mCherry-HIPP43 (*Hv*HIPP43 without isoprenylation motif) instead accumulated in the
319 nucleoplasm and at the plasma membrane. Moreover, co-expression with a plasma membrane
320 marker LTi6b-GFP and aniline blue staining confirmed its localisation at the plasma membrane
321 and loss of PD localisation (**Fig. S8C)** compared to the wild type (**Fig. S8D)**.

322

323 Given the strong interaction between Pwl2 and HIPP43 and the localisation of HIPP43 to PD,
324 we were keen to see the effect of co-expressing the effector and putative host target in the same
325 cells. When we co-expressed YFP-Pwl2 with mCherry-HIPP43, they co-localised in the
326 cytosol as mobile puncta approximately 2 µm in diameter (**Fig. 7I**). In some cases, we observed
327 larger mobile structures ranging from 2-4 µm in diameter (**Fig. 7I**). We also tested whether
328 Pwl1, Pwl3 and Pwl4 (**Fig. S9A**) could also co-localise with HIPP43 when co-expressed in *N.*
329 *benthamiana.* In the presence of Pwl1, HIPP43 PD localization was abolished, and the two
330 proteins co-localise in the cytoplasm and partially in cytoplasmic mobile structures (**Fig. S9B**)
331 Conversely, Pwl3 did not affect mCherry-HIPP43 localisation to PD (**Fig. S9C**), while Pwl4
332 (**Fig. S9D**) only showed cytoplasmic co-localisation without larger mobile bodies forming. In
333 addition, because we had observed that *Hv*HIPP43 orthologs from wheat (*Taes*HIPP43), foxtail
334 millet (*Siti*HIPP43) and weeping lovegrass (*Ec*HIPP43) interact with Pwl2 in Y2H assays, we
335 also tested whether *Taes*HIPP43, *Siti*HIPP43 or *Ec*HIPP43 localise as PD puncta in the same
336 way as *Hv*HIPP43. Interestingly, *Taes*HIPP43 (wheat) mostly localized to the nucleus,
337 cytoplasm and PD, even though PD localization was reduced (**Fig. S9E**), whereas *Ec*HIPP43
338 (weeping lovegrass) (**Fig. S9F**) and *Siti*HIPP43 (foxtail millet) **(Fig. S9G**) localized to small
339 puncta equivalent to PD, like *Hv*-HIPP43. Because Pwl2 is able to alter sub-cellular
340 localisation of *Hv*HIPP43, we tested whether this also occurred when *Siti*HIPP43 and Pwl2
341 were co-expressed. We observed Siti-HIPP43/Pwl2 co-localisation as cytoplasmic mobile
342 bodies away from PD, mirroring the Pwl2/HvHIPP43 interaction (**Fig. S9H-J**). When
343 considered together, we conclude that Pwl2 and its family members can interact with
344 *Hv*HIPP43 and that Pwl2 can also interact with HIPP43 orthologs from other cereals, thereby
345 altering their deployment to PD.

346 **Pwl2 consistently alters the plasmodesmatal localization of HIPP43.**

347 To understand the effect of Pwl2 expression on the PD localisation of *Hv*HIPP43, we carried
348 out a detailed quantitative analysis. In control experiments we expressed *Hv*HIPP43 with free
349 cytoplasmic YFP, and two MAX effectors AVR-PikE and MEP3 (Yan *et al.*, 2023). In six
350 independent co-expression experiments, we observed co-localisation of Pwl2 and *Hv*HIPP43
351 as mobile cytoplasmic puncta or large cytoplasmic mobile structures, while PD localisation
352 was significantly reduced (**Fig. 7I and J)**. By contrast, co-localisation of *Hv*HIPP43 with AVR-
353 PikE or MEP3 led to mCherry-*Hv*HIPP43 fluorescence remaining at PDs (**Fig. 7K-N)**.
354 Moreover, mCherry-HIPP43 fluorescence showed greater intensity when co-expressed with

355 Pwl2 compared to when co-expressed with AVR-PikE or MEP3 **(Fig. 7K-N)**. It is therefore
356 possible that Pwl2 is able to stabilise *Hv*HIPP43 or increases its accumulation, because the
357 mCherry-*Hv*HIPP43 signal is barely detectable in the absence of Pwl2 (**Fig. 7K and M)**. Our
358 previous structural analysis demonstrated that Pwl2 and *Os*HIPP43 produce a robust binding
359 interface that requires up to seven mutations in Pwl2 (*Pwl2*^{SNDEYWY}) to abolish (Zdrzałek *et*
360 *al.*, 2024). To test whether binding of Pwl2 to HIPP43 is necessary for the alteration in its
361 cellular localisation, we co-infiltrated mCherry-HIPP43 and YFP-Pwl2^{SNDEYWY} in *N.*
362 *benthamiana* and carried out live cell imaging. We were able to observe YFP-Pwl2^{SNDEYWY}
363 expression, but this did not alter mCherry-*Hv*HIPP43 localisation at PD (**Fig. 7O-P)**.
364 Furthermore, the fluorescence intensity of mCherry-*Hv*HIPP43 did not increase as it did upon
365 co-expression with YFP-Pwl2 **(Fig. 7I and O)**. To rule out the possibility that Pwl2 degrades
366 *Hv*HIPP43 upon interaction in plant cells, we carried out immuno-blot analysis using protein
367 extracts from *N. benthamiana* following co-infiltration of mCherry-HIPP43 with either Pwl2,
368 MEP3 or AVR-PikE. Strikingly, the presence of Pwl2 led to pronounced mCherry-*Hv*HIPP43
369 accumulation compared to when co-infiltrated with MEP3 or AVR-PikE **(Fig. 7Q)**. We were
370 also concerned that Pwl2/HIPP43 co-localisation as puncta could be mis-interpreted as also
371 occurring at PD. To rule out such a possibility, we stained PD with aniline blue after co-
372 infiltrating *Hv*HIPP43 with free-YFP, YFP-Pwl2, AVR-PikE-YFP and MEP3-YFP. In a
373 control experiment we expressed free-YFP, YFP-Pwl2, AVR-PikE-YFP and MEP3-YFP in the
374 absence of *Hv*HIPP43. We found that free-YFP, Pwl2, AVR-PikE-YFP and MEP3 show
375 localisation to the cytosol **(Fig. S10A-D**), but MEP3-YFP also showed some additional PD
376 localisation. By contrast YFP-Pwl2 was always observed as cytoplasmic mobile puncta (**Fig.**
377 **S10B**). When cells expressing Pwl2 were stained with aniline blue there was no co-localization
378 of Pwl2 and the aniline blue signal (**Fig. S10E-G**). In the presence of mCherry-HIPP43 and
379 YFP-Pwl2, co-localisation at cytoplasmic puncta/mobile bodies was observed and did not co-
380 localise with aniline blue staining (**Fig. S10H**)**.** In limited cases where co-localisation was
381 observed, this was transient because the Pwl2/HIPP43 puncta are mobile. By contrast, when
382 expressed on its own, or in the presence of free-YFP or two MAX-fold effectors AVR-PikE,
383 free-YFP and MEP3, mCherry-HIPP43 co-localised with aniline blue to PD (**Fig. S10I-K**). To
384 investigate the motility of HIPP43-Pwl2 puncta, we carried out time-lapse imaging using
385 confocal laser microscopy of aniline blue-stained *N. benthamiana* cells following co-
386 infiltration of mCherry-HIPP43 with YFP-Pwl2, MEP3-YFP, AVR-PikE-YFP or YFP-
387 Pwl2^{SNDEYWY}. Blue stained puncta equivalent to PD remained immobile while mCherry-
388 HIPP43/YFP-Pwl2 fluorescence was observed at mobile cytoplasmic structures (see **Movie S1**

389 and individual frames shown in **Fig. S11A)**. By contrast, co-localisation of mCherry-HIPP43
390 at aniline blue-stained PD was clearly visible and not altered by the presence two MAX-fold
391 effectors MEP3-YFP and AVR-PikE-YFP, YFP-Pwl2^{SNDEYWY} or of free-YFP (see **Movie S2-**
392 **S5**) and frames in **Fig S11B-E)**. When considered together, these results provide evidence that
393 Pwl2 interacts with HIPP43 altering its cellular location away from plasmodesmata.

394 **The ability of Pwl2 to bind HIPP43 is necessary for its avirulence and virulence functions.**
395 As the interaction between Pwl2 and HIPP43 appears to be critical for altering its sub-cellular
396 localisation to PD, we decided to test if this was also necessary for the role of Pwl2 in blast
397 disease. We therefore set out to see whether the *pwl2*^{SNDEYWY} allele could complement the
398 mutant phenotypes of a *M. oryzae Δpwl2* mutant. To do this, we transformed *Δpwl2* mutant
399 with a construct expressing Pwl2^{SNDEYWY} under its native promoter (*PWL2p:pwl2*^{SNDEYWY}) and
400 successful transformants were selected (**Fig. 8A and B**). We then quantified *Pwl2*^{SNDEYWY} gene
401 expression in selected transformants using qRT-PCR (**Fig. 8C**). We reasoned that if recognition
402 of Pwl2 by Mla3 requires HIPP43 recognition (Gómez De La Cruz *et al*., 2024), then
403 Pwl2^{SNDEYWY} should not complement the observed gain of virulence of *Δpwl2* mutants on
404 barley cv. Baronesse (+*Mla3*). Moreover, if the Pwl2/HIPP43 interaction is required for the
405 virulence function of Pwl2, then Pwl2^{SNDEYWY} should not restore virulence to *Δpwl2* mutants.
406 In three independent experiments of two independent strains, C6 (*Δpwl2+PWL2p:pwl2*^{SNDEYWY})
407 and C14 (*Δpwl2+PWL2p:pwl2*^{SNDEYWY}) showed a compatible interaction on cv. Baronesse (**Fig.**
408 **8D)** providing evidence that the Pwl2^{SNDEYWY} is not recognised by Mla3, because the strains
409 retained the ability to infect a susceptible barley cv. Nigrate (-*Mla3*) (**Fig. 8E)**. We also
410 observed that *Δpwl2 +PWL2p:Pwl2*^{SNDEYWY} transformants C6 and C14 did not restore full
411 virulence on susceptible rice cv. CO39 compared to the wildtype Guy11 (**Fig. 8F**), based on
412 lesion density (**Fig. 8G)** and lesion length (**Fig. 8H)**. We conclude that the interaction between
413 Pwl2 and HIPP43 is required for both its recognition as an avirulence factor and its function as
414 a virulence determinant.
415
416

417 **Discussion**

418 The Pwl2 effector was first identified as a host specificity determinant for infection of the
419 forage grass species weeping lovegrass (Kang *et al.*, 1995; Sweigard *et al.*, 1995). Its initial
420 identification provided evidence that host range in plant pathogenic fungi was conditioned in
421 a similar way to cultivar specificity in a gene-for-gene manner, involving dominant pathogen
422 genes recognised by the products of cognate disease resistance genes (Kang *et al.*, 1995).
423 Furthermore, Pwl2 was found to belong to an expanded gene family, suggesting an important
424 function in pathogenicity and fitness (Kang *et al.*, 1995). However, in the following two
425 decades, the function of Pwl2 remained elusive despite its extensive use as a marker in cell
426 biological studies for investigating effector regulation, secretion and delivery during plant
427 infection (Kankanala *et al.*, 2007; Giraldo *et al.*, 2013; Oliveira-Garcia *et al.*, 2023b).
428
429 In this study, we set out to explore the function of Pwl2 and investigate why it is such a highly
430 conserved effector in *M. oryzae*. We found that *PWL2* is highly conserved in *M. oryzae*,
431 including each of its host-limited forms and even in sister *Magnaporthe* species infecting
432 crabgrass and pearl millet. The observation that *PWL2* and the wider *PWL* family genes have
433 been maintained in the global blast population and there are effector variants in certain host-
434 adapted lineages, suggests that Pwl2 and members of this family serve an important function
435 in pathogenesis. Furthermore, *PWL2* is present at high copy number in many *M. oryzae* isolates
436 having undergone extensive gene duplication and is specifically expressed during the initial
437 stages of blast infection, particularly at the stage when *M. oryzae* moves from an initially
438 colonised epidermal cell, following appressorium penetration, to adjacent host cells. This cell-
439 to-cell movement by the fungus utilises PD-containing pit fields and the fungus forms a
440 transpressorium structure that undergoes severe hyphal constriction to traverse each pit field
441 (Kankanala *et al.*, 2007; Cruz-Mireles *et al.*, 2021), a process that requires activity of the Pmk1
442 MAP kinase (Sakulkoo et al., 2018). We found that *PWL2* is expressed during this process in
443 a Pmk1-dependent manner, forming part of a regulated set of effectors deployed by the fungus
444 during cell-to-cell movement. The generation of a *Δpwl2* mutant, made possible by
445 CRISPR/Cas9 gene editing to delete all three native copies of the gene, enabled us to confirm
446 the role of Pwl2 in host specificity to weeping lovegrass (Sweigard et al., 1995), as an
447 avirulence effector for barley Mla3 (Brabham et al., 2024), and also revealed its importance in
448 blast disease. Pwl2 is therefore an important virulence determinant for blast disease, explaining
449 its conservation and amplification.

450 To identify the likely target of Pwl2, we utilised discovery proteomics which revealed its
451 interaction with an isoprenylated small HMA protein, HIPP43. This is consistent with Pwl2
452 being a MAX effector – many of which have been shown to interact with sHMA protein
453 domains – although previous studies have focused on incorporation of sHMA domains into
454 paired NLR immune receptors leading to disease resistance (Ortiz *et al.*, 2017; Bentham *et al.*,
455 2021; Maidment *et al.*, 2021; Mukhi *et al.*, 2021). The crystal structure of the Pwl2/HIPP43
456 complex (Zdrzałek *et al.*, 2024) demonstrates that Pwl2 uses an expansive interface to mediate
457 binding to HIPP43, largely using elements of the MAX fold to interact with the β-sheet of its
458 host target. Indeed, when HIPP43 is incorporated into the Pik-1 NLR, in place of its naturally
459 occurring integrated HMA domain, this leads to an immune response to Pwl2 (Zdrzałek *et al.*,
460 2024). A recent study has also revealed that the barley resistance protein Mla3 acquired the
461 ability to bind Pwl2 by mimicking the HMA fold of its host target, HIPP43 (Gómez De La
462 Cruz *et al.*, 2024). Interestingly, polymorphic residues found in Pwl2 variants, such as pwl2-2
463 and pwl2-3 are not located at the HIPP43 binding interface but are located away from the MAX
464 fold in the C-terminal helix of Pwl2. It is possible that these polymorphic residues are essential
465 to stabilize the Pwl2, MAX-fold/HMA-like interface in Mla3. Consistent with this idea,
466 introducing mutations that disrupt the Pwl2/HIPP43 interaction also results in loss of
467 recognition by Mla3.
468
469 In spite of the importance of sHMA domains in plant immunity, little is known regarding their
470 actual function or why they are targeted by fungal effectors. HMA domains are known to be
471 involved in biotic/abiotic stress responses, transport of metals and metal detoxification, and
472 their expression can be organ-specific or tissue-specific within roots, leaves, or stems (Barth *et*
473 *al.*, 2009; Zschiesche *et al.*, 2015; Zhang *et al.*, 2020). Moreover, sHMAs can localize to the
474 nucleus, plasma membrane, cytoplasm, or to plasmodesmata (Barth *et al.*, 2009; Cowan *et al.*,
475 2018; Barr *et al.*, 2023; Oikawa *et al.*, 2024). Furthermore, sHMAs are expanded in plant
476 genomes with more than 45, and more than 50, sHMA domain-encoding genes occurring in
477 *Arabidopsis* and rice, respectively (de Abreu-Neto *et al.*, 2013). Unique intragenic deletions in
478 OsHIPP05 (*Pi21*), a proline rich HMA domain protein-encoding gene in rice leads to rice blast
479 resistance (Fukuoka *et al.*, 2009) and gene silencing or deletion mutants of *TaHIPP1* or
480 *AtHMAD1* in wheat and *Arabidopsis* provide enhanced resistance against *Puccinia striiformis*
481 f. sp. *tritici* and *Pseudomonas syringae* DC3000, respectively (Imran *et al.*, 2016; Wang *et al.*,
482 2023). In addition, deletion mutants of *AtHIPP27* in *Arabidopsis* lead to increased resistance
483 against cyst nematodes (Radakovic *et al.*, 2018). However, it is not clear why deletion of sHMA

484 protein-encoding genes impacts immunity. Therefore, the observation that Pwl2 interacts with
485 HIPP43 is revealing, especially because over-expression of either Pwl2 or *Hv*HIPP43
486 suppresses PTI responses and enhances blast disease susceptibility. How this potential
487 enhancement of HIPP43 activity is stimulated by Pwl2 is not completely clear, but transient
488 co-expression of both Pwl2 and HIPP43 sequesters HIPP43 away from plasmodesmata (PD),
489 and the two proteins instead co-localize in large mobile structures within the cytoplasm. The
490 localisation of HIPP43 to PD requires its isoprenylation motif and may be associated with an
491 immune signaling role at this site. Given the Pmk1 MAP kinase-dependent expression of Pwl2
492 during PD traversal, it may be that sequestering HIPP43 away from these sites is critical for
493 the fungus to invade plant tissue efficiently. This is consistent with the reduced virulence
494 phenotype of *Δpwl2* mutants, which results in slower generation of disease symptoms and
495 reduced lesion size. A recent study has highlighted how a *P. infestans* effector PiE354 can
496 interfere with a host immune response by re-routing a plant Rab8a away from the
497 plant/pathogen interface, a similar potential effector function that alters the cellular location of
498 a target rather than impairing a particular function (Yuen *et al.*, 2024).
499
500 Localization of two HIPP proteins, HIPP7 and HIPP26, to PD has been previously reported,
501 which is also dependent on isoprenylation motifs like HIPP43 (Cowan *et al.*, 2018; Guo *et al.*,
502 2021). Although characterized HIPPs have been proposed to be metallochaperones, there are
503 no studies that link metal detoxification to immunity. Some studies suggest that there may be
504 a connection between concentration of metal ions, such as iron, copper, cadmium and zinc,
505 with plasmodesmatal permeability (O'Lexy *et al.*, 2018), which might explain the function of
506 a plasmodesmatal localized HIPP in regulating permeability, associated with their role in
507 immunity. Both the HMA domain and isoprenylation regions of HIPPs have been shown to be
508 important for plant immunity. For example, a mutation targeting the proline-rich region of *pi21*
509 is sufficient to lead to gain of resistance against *M. oryzae* (Fukuoka *et al.*, 2009), while
510 interfering with the isoprenylation of HIPP1-V from wild wheat (*H. villosa*) leads to loss of
511 resistance against *Blumeria graminis* f. sp. *tritici* accompanied by reduced HIPP1-V
512 localization to plasma membrane. Interestingly, HIPP1-V interacts with the E3-ligase CMPG1-
513 V at the plasma membrane leading to resistance to powdery mildew in an isoprenylation-
514 dependent manner (Wang *et al.*, 2023). This interaction has been reported to activate
515 expression of genes involved in ROS generation and salicylic acid biosynthesis, suggesting
516 that HIPP1-V is required for PTI regulation (Wang *et al.*, 2023). Interestingly, we found that

517 HIPP1-V is an ortholog of HvHIPP43 and can interact with Pwl2 in a Y2H assay. It is possible,
518 therefore, that the Pwl2 interaction with HvHIPP43 attenuates PTI through a similar
519 mechanism, which will require further investigation.
520
521 How the change in cellular localization of HIPP43 induced by the Pwl2 effector prevents its
522 function in immunity or leads to a new role that enhances disease susceptibility remains
523 unclear. A very recent study has provided evidence that *M. oryzae* AVR-Pik binding stabilizes
524 the rice small HMA (sHMA) proteins OsHIPP19 and OsHIPP20 (Oikawa *et al.*, 2024),
525 suggesting that the function of Pwl2 may be mirrored by other blast effectors, targeting a wider
526 pool of HIPPs. In this regard, future work will be necessary to determine whether HIPP43
527 directly regulates ROS generation, which might reduce permeability of plasmodesmata (Cui
528 and Lee, 2016), or acts in a more indirect manner through interaction with other signaling
529 components involved in PTI. Finally, Pwl2 is known to be a highly mobile effector and has
530 been shown to move into neighbouring rice cells ahead of *M. oryzae* hyphal growth (Giraldo
531 *et al.*, 2013). This has been suggested to be a step to prepare un-invaded cells for fungal
532 colonisation, consistent with its Pmk1-dependent regulation. Pwl2 may therefore alter the sub-
533 cellular localisation and concentration of HIPP43, sequestering it away from PD that the fungus
534 uses for effector movement and hyphal invasion, thereby enabling more rapid tissue
535 colonisation by the blast fungus.
536

537 **Materials and methods**

538 **Fungal strains, growth conditions and infection assays**

539 Fungal isolates were routinely grown on complete medium (CM) at 24°C with a controlled 12
540 h light and dark cycle for up to 12 days (Talbot *et al.*, 1993). *H. vulgare*, *E. curvula* and *O.*
541 *sativa* plants were grown for 7, 14 and 21 days respectively in 9 cm diameter plastic plant pots
542 or seed trays. Conidia were recovered from 10-day old cultures using a sterile disposable plastic
543 spreader in 3 mL sterile distilled water. The conidial suspension was filtered through sterile
544 Miracloth and centrifuged at 5000 x g for 5 min at room temperature before adjusting to a final
545 of concentration of 1 x10^5 conidia mL^{-1} in 0.2 % gelatin. The spore suspension was used for
546 spray or leaf drop infections assays. After spray inoculation, plants were placed in polythene
547 bags and incubated in a controlled plant growth chamber at 24°C for 48 h with a 12 h light-
548 dark cycle and 85% relative humidity, before removing polythene bags. Inoculated plants were
549 incubated for 3 days before scoring lesions. For each treatment 10 leaves were collected before
550 counting typical ellipsoid necrotic disease lesions with a grey centre (Valent *et al.*, 1991). Each
551 experiment was repeated a minimum of three times, yielding consistent outcomes.

552 **Leaf infection assay and live-cell imaging**

553 Rice leaf sheath from 4 week old susceptible cultivars Moukoto or CO39 were inoculated with
554 4 mL of a suspension at 5 x 10^4 conidia mL^{-1} in ddH2O using a micropipette (Kankanala *et al.*,
555 2007). Inoculated leaf sheaths were incubated at 24°C for 24 h before a thin layer of inner leaf
556 sheath was dissected and mounted on a glass slide. Treatment with INA-PP1 was carried as
557 described previously (Sakulkoo *et al.*, 2018). Live cell imaging was carried out on an IX81
558 motorized inverted microscope (Olympus, Hamburg, Germany) for conventional and
559 differential interference contrast (DIC) microscopy using Photometrics CoolSNAP HQ2
560 camera (Roper Scientific, Germany). Images were analyzed using ImageJ. For Leica SP8 laser
561 confocal microscopy, settings were as follows; GFP, YFP and RFP/mCherry tagged proteins
562 were excited using 488, 514 and 561 nm laser diodes and emitted fluorescence detected using
563 495-550, 525-565 and 570-620 nm respectively. Auto-fluorescence from chlorophyll was
564 detected at 650-740 nm.

565 **Generation of fungal transformation plasmids**

566 Single or multiple DNA fragments were cloned into fungal transformation vectors using In-
567 Fusion HD Cloning (Clontech, USA). Briefly, fragments from cDNA, genomic DNA or
568 synthesized DNA were amplified using primers to introduce a 15bp overhang complementary

569 to sequences at restriction sites of a destination vector or adjacent insert fragments. This allows
570 the ends to fuse by homologous recombination. Positive transformants were selected by colony
571 PCR and constructs sequenced by GENEWIZ. A list of primers is provided in Table S3.

572 **RNA isolation, RNA sequencing and analysis**

573 To study *in-planta* gene expression of *PWL2* and other effectors, leaf drop infection assays
574 were carried out using susceptible rice cv. Moukoto and samples collected at 24 and 72 hpi.
575 Infected plant material was ground to a fine powder using a sterile nuclease-free mortar &
576 pestle containing liquid N_2. RNA was isolated from *M. oryzae* mycelium, or inoculated rice
577 leaves using QIAGEN RNeasy Plant Mini Kit. RNA quality was determined NanoDrop
578 spectrophotometry (Thermo Scientific, UK) and Agilent 2100 Bioanalyser (Agilent
579 Technologies, UK). Library preparation was carried out using Illumina® sequencing TruSeq
580 Stranded Total RNA Library Prep Kit before sequencing 100 bp paired ends reads using
581 Illumina Genome Analyser GXII platform by Exeter Sequencing Service (University of
582 Exeter). To determine differential gene expression, raw reads were separated by mapping to
583 both *M. oryzae* and *O. sativa* using kraken2. Reads specific to *M. oryzae* were used to quantify
584 transcript abundance using Kallisto. To quantify genes missing in 70-15, separated reads were
585 mapped to KE002. R package Sleuth was used to determine genes showing differential
586 expression with log2fold > 1 and P-adjust value < 0.05 defined as up-regulated and a log2fold
587 > 1 and P-adjust value < 0.05 as down-regulated. Southern blot analysis of *M. oryzae* genomic
588 DNA was carried out as described previously (Talbot *et al.*, 1993). Quantitative real-time PCR
589 was carried out using CFX OPUS 96 and CT values normalised to a house keeping gene, β-
590 Tubulin (MGG_00604). Fold change was determined using the formula $2^{-\Delta\Delta CT}$, where ΔΔCt =
591 ((CtGOI in infected sample - CtNC in infected sample) – (CtNC in mycelia - CtNC in
592 mycelia)), and GOI is the gene of interest and NC (negative control) is β-Tubulin.

593 **Generation of Cas9-sgRNA targeted gene deletion**

594 A sgRNA was designed for CRISPR-Cas9 genome editing using online tool E-CRISP
595 http://www.e-crisp.org/E-CRISP/. A 20-nucleotide sequence was selected at the *PWL2* locus
596 (not including the PAM NGG-sequence). The sgRNA was first synthesised using the EnGen
597 sgRNA synthesis kit New England Biolabs (NEB #E3322) before mixing with Cas9-NLS to
598 form an RNP complex (Foster *et al.*, 2018). The mixture was incubated at room temperature
599 for 10 min before fungal transformation. *M. oryzae* protoplasts were generated as described
600 previously (Talbot *et al.*, 1993). The RNP complex together with donor template was mixed

601 with Guy11 protoplasts re-suspended in 150 µL STC to a concentration of $1x10^8$ mL^{-1}
602 incubated at room temperature for 25 min before adding 60% PEG. Successful transformants
603 were selected on complete medium (CM) agar containing 200 µg mL^{-1}Hygromycin B .

604 **Whole genome sequencing**

605 Purified RNA-free DNA was obtained using Hexadecyltrimethylammonium Bromide
606 (CTAB). Template quality was assessed by NanoDrop and Qubit spectrophotometry.
607 Sequencing was carried out at Exeter Sequencing services (University of Exeter, UK) and
608 Novogene (Cambridge, UK). NEXTflex™ Rapid DNA-seq Library Prep Kit was used to
609 prepare and index libraries before sequencing on HiSeq 2500 (Illumina) with two lanes per
610 sample. Quality of sequencing reads was checked using FastQC
611 (http://www.bioinformatics.bbsrc.ac.uk/projects/fastqc/). From raw data (fastq files), adaptor
612 sequences were trimmed from sequences containing adaptors and low-quality reads removed
613 by fastq-mcf. Trimmed sequences were aligned to the reference genome (70-15) (Dean *et al.*,
614 2005) using BWA (Burrow Wheeler Aligner) https://github.com/lh3/bwa (Li and Durbin,
615 2009). Bam files were visualized by IGV genome viewer to determine CRISPR gene deletion.

616 **Copy number variation of *PWL2***

617 A total of 286 *M. oryzae* isolates with raw Illumina-based sequencing information were
618 downloaded from NCBI (performed on October 16th, 2019). Copy number variation was
619 assessed using a k-mer analysis approach using the k-mer analysis toolkit (KAT; v2.4.1).
620 Coding sequence information for *M. oryzae* isolate 70-15 was used as template for k-mer
621 analysis and raw Illumina reads were input. Default parameters were used including k-mer
622 length 27 nt. Copy number variation of individual effectors is based on average k-mer coverage
623 compared with the median coverage for all genes.

624 **Phylogenetic analysis of *Magnaporthe* isolates**

625 Genome sequences of diverse *M. oryzae* isolates were identified by literature review and
626 searches on NCBI (performed August 9th, 2019). For isolates having only Illumina sequencing
627 data, raw paired reads were downloaded from NCBI, trimmed using Trimmomatic (v0.36)
628 using the parameters: removal of adapters with ILLUMINACLIP:TruSeq2-PE.fa:2:30:10,
629 remove leading low quality or N based with quality below 5 for leading (LEADING:5) and
630 trailing sequence (TRAILING:5), scan and cut reads with 4 bp sliding window below 10
631 (SLIDINGWINDOW:4:10), and minimum length 36 bp (MINLEN:36). KmerGenie (v1.7048)
632 was used to identify an optimal k-mer for genome assembly using default parameters. Genome

633 assembly was performed using minia (v0.0.102) with default parameters. kSNP3 (v.3.021) was
634 used to develop a phylogenetic tree of *M. oryzae* using assembled genomes as input with
635 parameters of k-mer of 29 bp and minimum fraction of 0.4. The phylogenetic tree was
636 generated using RAxML (v8.2.12) using the General Time Reversible model of nucleotide
637 substitution under the Gamma model of rate heterogeneity.

638 **Generation of *Agrobacterium* transformation plasmids**

639 Single or multiple DNA fragments were cloned into binary vectors using In-Fusion HD
640 Cloning (Clontech, USA). Briefly, fragments from cDNA were amplified to introduce a 15bp
641 overhang complementary to sequences at restriction sites of a destination vector or adjacent
642 insert fragments. Alternatively, synthesized DNA fragments were designed with a 15bp
643 overhang complementary to sequences at restriction sites of binary vector pG514 customized
644 for infusion cloning by digestion by either *Xba*I and *Pca*I or *Sac*I (New England Biolabs) to
645 remove the *ccDB* toxin encoding gene. Positive transformants were accessed by colony PCR
646 and constructs sequenced and analyzed on SNAP gene.

647 **Transient expression in *Nicotiana benthamiana***

648 *Agrobacterium tumefaciens* strain *GV3101* (Holsters *et al.*, 1980) was used for transient
649 expression. Three-week-old *N. benthamiana* leaves were infiltrated with transformed
650 *Agrobacterium* carrying T-DNA constructs expressing the gene of interest. Bacterial cultures
651 were diluted to obtain a final OD_{600} of 0.4 in agroinfilitration buffer (10mM MES, 10 mM
652 $MgCl_2$, 150 µM acetosyringone, pH 5.6). Leaf discs were cut from agroinfiltrated tissue 48 hpi
653 and subjected for microscopy or used for co-IP.

654 **Plant transformation and ROS measurement**

655 *Agrobacaterium tumefaciens* strain *AGL1* (Holsters *et al.*, 1980) was used for plant
656 transformation (Hensel *et al.*, 2009). Positive transgenic plants were selected on HygromycinB
657 followed by confirmation using PCR. Alternatively, leaf discs were collected from transgenic
658 plants and analysed for copy number by iDNA Genetics Ltd (Norwich, UK). In addition,
659 expression of the protein was evaluated using SDS-PAGE. To measure the response to PTI
660 elicitors, a 4-mm diameter biopsy punch (Integra™ Miltex ™) was used to cut leaf discs from
661 5-week-old *H. vulgare* transgenic plants. Leaf discs were transferred to 96-well-plates (Greiner
662 Bio-One) containing 100 µL ddH_2O in each well and incubated overnight at room temperature.
663 The assay was carried out by replacing ddH_2O in wells by a 100 µL of 100 µM Luminol or L-
664 012 (Merck), 20 µg mL^{-1} horseradish peroxidase (Merck) together with elicitors, flg22 (1 µM

665 final concentration), chitin (1mg/mL final concentration) or without (mock). Photon count was
666 carried out using a HRPCS218 (Photek) equipped with a 20 mm F1.8 EX DG ASPHERICAL
667 RF WIDE LENS (Sigma Corp). Each experiment was repeated three times, yielding consistent
668 outcomes.

669 **Co-immunoprecipitation and sample preparation for mass spectrometry**

670 Leaves were harvested from 14-21 day old barley transgenic plants and rapidly frozen in liquid
671 N_2 before storage or immediately ground to fine powder using a GenoGrinder® tissue
672 homogenizer. Ground powder was quickly transferred to ice-cold 1.5 mL Eppendorf tubes and
673 2 mL of ice-cold extraction buffer (GTEN [10% (v/v) glycerol, 25 Mm Tris pH 7.5, 1 mM
674 EDTA 150 mM NaCl, 2% (w/v) PVPP, 10 Mm DTT, 1 X protease inhibitor cocktail (Sigma),
675 0.5% (v/v) IGEPAL added and mixed thoroughly. This was centrifuged at 3000 x g for 10 min
676 at 4°C to recover total protein in the supernatant and repeated twice. A volume of 2 mL of total
677 protein was mixed with 25 µL of GFP-TRAP agarose beads (50% slurry, ChromoTek) and
678 incubated shaking overnight at 4°C. The GFP-TRAP agarose beads were centrifuged for 2 min
679 at 3000 x g before washing three times with wash buffer (ChromoTek). Bound proteins were
680 recovered by resuspending beads in loading buffer (loading dye, 10 mM DTT, H2O) before
681 incubating at 70°C for 10 min. An aliquot was run by SDS-PAGE and used for immuno-blot
682 analysis (Burnette, 1981). Recovered proteins were fractionated by SDS-PAGE for
683 approximately 1 cm. The gel was washed for 1 h in ddH_2O followed by 1 incubation
684 SimplyBlue™ Safe stain. The gel was then washed three times in ddH_2O and the region
685 containing proteins excised using a scalpel.

686 **Mass spectrometry and data processing**

687 Protein purification, immunoprecipitation, sample preparation, liquid chromatography
688 followed by tandem mass spectrometry (LC-MS/MS), and data analysis were carried out as
689 previously described (Li *et al.*, 2023). Proteins identified in immunoaffinity-enriched samples
690 were measured by high resolution LC-MS systems, Orbitrap Fusion (Thermo Ltd). Acquired
691 spectra were peak-picked and searched by Mascot (Matrix Science Ltd) to identify peptide
692 sequences from the search space defined by background proteome. Peptides were combined
693 into proteins based on the principle of parsimony by the search engine. Resulting proteins were
694 further described by quantitative values based on the number of spectra that identify them.
695 Individual runs were combined in Scaffold (Proteome Software Inc.), where the data were
696 evaluated and filtered to contain less than 1% false positives (FDR) and the resulting matrix

697 exported. The matrix of proteins detected in different samples serves as the input for an R script
698 for further processing and visualization.

699 **Yeast two-hybrid analysis**

700 To clone genes of interest into bait (pGBKT7 DNA-BD cloning) vector or prey (pGADT7
701 activating domain) vector, by In-Fusion HD Cloning (Clontech), bait and prey vectors were
702 digested by *Bam*H1 and *Eco*R1 while gene to be inserted was PCR-amplified using primers
703 containing 15 bp overhangs with homology to two ends of the digested bait vector. For
704 transformation, a single colony Y2H gold yeast strain was mixed in 1 mL of liquid yeast extract
705 peptone dextrose (YPD). Competent cells were prepared according to manufacturer
706 instructions (Zymo Research). Briefly, for transformation 700 ng – 1 µg of plasmids expressing
707 Pwl2 or other effectors in pGADT7 and *Hv*HIPP43 or plant proteins in pGBKT7 were co-
708 transformed in competent cells and Frozen-EZ Yeast Solution 3 added before incubation at
709 28°C for 1 h and transformed cells plated on selection media lacking Leucine (L) and
710 Tryptophan (W) and incubated at 28° C for 3-5 days. To detect interactions colonies were
711 transferred to media lacking Leucine (L), Tryptophan (W), Adenine (A) Histidine (H), Bromo-
712 4-Chloro-3-Indolyl a-D-galactopyranoside (X-a-gal) and 10 mM 3-amino-1,2,4-triazole (3AT)
713 (Sigma). The plates were imaged after 60-72 incubation at 28°C. Each experiment was
714 conducted a minimum of three times.

715 ***In-planta* co-immunoprecipitation (co-IP)**

716 To test interactions of proteins *in planta*, genes of interest tagged with either GFP or Myc were
717 cloned into vector pGW514, transformed into *Agrobacterium* strain *GV3101* and co-infiltrated
718 (OD_{600} = 0.4 for effectors and OD_{600} = 0.6 for HIPP43) into 3-4 week-old *N. benthamiana*
719 leaves and incubated for 48 h to allow protein expression. Total protein was isolated in ice-
720 cold extraction buffer (GTEN [10% (v/v) glycerol, 25 Mm Tris pH 7.5, 1 mM EDTA 150 mM
721 NaCl], 2% (w/v) PVPP, 10 Mm DTT, 1 X protease inhibitor cocktail (Sigma), 0.5% (v/v)
722 IGEPAL). Total protein was co-immunoprecipitated using anti-GFP M2 resin (Sigma-Aldrich,
723 St. Louis, MO) and washed 3 times using immunoprecipitation buffer before analyzing by
724 SDS-PAGE. Recovered proteins from co-immunoprecipitation were separated by SDS-PAGE
725 and transferred to a polyvinylidene diflouride (PVDF) membrane using a Trans-Blot turbo
726 transfer system (Bio841 Rad, Germany). Detection was performed using the appropriate
727 antibody either anti-GFP-HRP or anti-Myc-HRP. Imaging was carried out using an

728 ImageQuant LAS 4000 luminescent imager (GE Healthcare 844 Life Sciences, Piscataway,
729 NJ, U.S.A.) according to manufacturer's instructions.

730 **Sub-cellular localization and plasmodesmata quantification**

731 Leaf discs were obtained from *N. benthamiana* plants agroinfiltrated with different construct
732 combinations at 24 and 48 hpi and mounted on a slide immersed in perfluorodecalin and
733 observed using X63 oil immersion lens. For Leica SP8 laser confocal microscopy, settings
734 were as follows; GFP, YFP and RFP/mCherry tagged proteins were excited using 488, 514,
735 and 561 nm laser diodes and emitted fluorescence detected using 495-550, 525-565, and 570-
736 620 nm respectively. Auto-fluorescence from chlorophyll was detected at 650-740 nm. To stain
737 and quantify plasmodesmata (PD), agroinfiltrated leaves were further infiltrated with 0.1%
738 aniline (Sigma-Aldrich #415049, in PBS buffer, pH 7). Images were analyzed using ImageJ to
739 determine the number of PD. First, cell peripheries were divided into 20 µm sections and the
740 number of PD determined per 20 µm.

741 **Phylogenetic analysis of grass HMA proteins**

742 Proteins from *B. distachyon* (314; v3.1), *H. vulgare* (Barley cv. Morex V3, Jul 2020), *T.*
743 *aestivum* (RefSeqv2.1; 09-16-2020), *O. sativa* (323; v7.0), *Oropetium thomaeum* (386; v1.0),
744 *Sorghum bicolor* (454; v3.1.1), *Setaria italica* (312; v2.2), and *Zea mays* (RefGen_V4)
745 containing an HMA domain were identified using InterProScan (v5.59-91.0; Pfam PF00403).
746 The HMA domain was extracted using the script QKdomain_process.py
747 (https://github.com/matthewmoscou/QKdomain) including an additional 10 amino acid
748 sequences N and C-terminal of the Pfam boundaries (-n 10 -c 10). The non-redundant set of
749 HMA domains were identified using CD-HIT (v.4.8.1) with parameter -c 1.0. Structure-guided
750 multiple sequence alignment was performed using MAFFT with parameters dash, max iteration
751 of 1000, and globalpair. Maximum likelihood phylogenetic analysis was performed using
752 RAxML (v8.2.12) using the Gamma model of rate heterogeneity, JTT amino acid substitution
753 model,- and 1,000 bootstraps. Coding sequence was identified for the HIPP43 gene family and
754 aligned using MUSCLE (v5) translation alignment using default parameters. Maximum
755 likelihood phylogenetic analysis was performed using RAxML (v8.2.12) using General Time
756 Reversible model of nucleotide substitution under the Gamma model of rate heterogeneity and
757 1,000 bootstraps.
758

759 **Statistical analysis and Protein Structure Prediction**

760 Significance difference between groups of samples was performed using GraphPad Prism 10.
761 P values < 0.05 were considered significant, ****P<0.0001, ***P<0.001, **P<0.01 while
762 values P values > 0.05 were considered as non-significant in an unpaired Student's t-test.
763 Structure prediction was carried out using AlphaFold3 (Abramson *et al.*, 2024), the structure
764 analyzed and figures generated using ChimeraX (Meng *et al.*, 2023).

765

766 **Acknowledgements**

767 We thank current and past members of the "BLASTOFF" team from the Banfield, Kamoun,
768 Terauchi, Talbot, and Moscou Laboratories. For funding, we thank Gatsby Charitable
769 Foundation and Biotechnology and Biological Sciences Research Council (BBSRC)
770 BBS/E/J/000PR9797 and a BBSRC grant to NJT and FLHM (BB/V016342/1), United States
771 Department of Agriculture-Agricultural Research Service CRIS #5062-21220-025-000D
772 (MJM) and BB/X010996/1, funding for APH ISP. We acknowledge Y.K Gupta, J.C De la
773 Concepcion, J. Rhodes and J. Win for constructive discussions.

774

775 **Author Contributions**

776 **Conceptualization:** NJT and VW

777 **Formal analysis:** VW, XY, AF, JK, JS, DG, TL, YPH, ABE, MS, MJB, MM, WM and RZ

778 **Funding acquisition:** NJT

779 **Investigation** VW, XY, AF, JS, DG, AG, NS, DK, YPH, ABE, MJB, WM and RZ

780 **Writing – original draft:** VW and NJT

781 **Writing – review & editing:** VW, NJT, LR, AB, TL, MB, SK, MM, FM

782

ORCID IDs

Vincent Were:	0000-0002-9885-4877
Xia Yan:	0000-0003-4509-0137
Andrew J. Foster:	0000-0002-8459-7590
Jan Sklenar:	0000-0003-1858-2574
Thorsten Langner:	0000-0002-3401-8888
Amber Gentle:	0009-0006-1944-4754
Neha Sahu	0009-0008-0721-6337
Adam R. Bentham:	0000-0001-5906-0962
Rafał Zdrzałek:	0000-0003-3669-924X
Lauren Ryder:	0000-0003-0370-5746
Davies Kaimenyi:	0000-0002-6320-3740
Diana Gómez De La Cruz:	0000-0001-6683-9245
Yohann Petit-Houdenot:	0000-0003-4806-8349
Alice Bisola Eseola:	0000-0001-5698-8204
Mark Jave Bautista:	0000-0002-6016-5953
Weibin Ma:	0000-0002-0516-2151
Jiorgos Kourelis:	0000-0002-9007-1333
Dan MacLean:	0000-0003-1032-0887
Mark J. Banfield:	0000-0001-8921-3835
Sophien Kamoun:	0000-0002-0290-0315
Frank L.H.Menke:	0000-0003-2490-4824
Matthew J. Moscou:	0000-0003-2098-6818
Nicholas J Talbot:	0000-0001-6434-7757

References

Abramson, J., Adler, J., Dunger, J., Evans, R., Green, T., Pritzel, A., Ronneberger, O., Willmore, L., Ballard, A.J., Bambrick, J., Bodenstein, S.W., Evans, D.A., Hung, C.C., O'Neill, M., Reiman, D., Tunyasuvunakool, K., Wu, Z., Žemgulytė, A., Arvaniti, E., Beattie, C., Bertolli, O., Bridgland, A., Cherepanov, A., Congreve, M., Cowen-Rivers, A.I., Cowie, A., Figurnov, M., Fuchs, F.B., Gladman, H., Jain, R., Khan, Y.A., Low, C.M.R., Perlin, K., Potapenko, A., Savy, P., Singh, S., Stecula, A., Thillaisundaram, A., Tong, C., Yakneen, S., Zhong, E.D., Zielinski, M., Žídek, A., Bapst, V., Kohli, P., Jaderberg, M., Hassabis, D., and Jumper, J.M. (2024). Accurate structure prediction of biomolecular interactions with AlphaFold 3. Nature **630,** 493-500.

Ashikawa, I., Hayashi, N., Yamane, H., Kanamori, H., Wu, J., Matsumoto, T., Ono, K., and Yano, M. (2008). Two Adjacent Nucleotide-Binding Site–Leucine-Rich Repeat Class Genes Are Required to Confer Pikm-Specific Rice Blast Resistance. Genetics **180,** 2267-2276.

Asuke, S., Tanaka, M., Hyon, G.S., Inoue, Y., Vy, T.T.P., Niwamoto, D., Nakayashiki, H., and Tosa, Y. (2020). Evolution of an Eleusine-Specific Subgroup of Pyricularia oryzae Through a Gain of an Avirulence Gene. Mol Plant Microbe Interact **33,** 153-165.

Barr, Z.K., Werner, T., and Tilsner, J. (2023). Heavy Metal-Associated Isoprenylated Plant Proteins (HIPPs) at Plasmodesmata: Exploring the Link between Localization and Function. In Plants.

Barth, O., Vogt, S., Uhlemann, R., Zschiesche, W., and Humbeck, K. (2009). Stress induced and nuclear localized HIPP26 from Arabidopsis thaliana interacts via its heavy metal associated domain with the drought stress related zinc finger transcription factor ATHB29. Plant Molecular Biology **69,** 213-226.

Bentham, A.R., Petit-Houdenot, Y., Win, J., Chuma, I., Terauchi, R., Banfield, M.J., Kamoun, S., and Langner, T. (2021). A single amino acid polymorphism in a conserved effector of the multihost blast fungus pathogen expands host-target binding spectrum. PLoS Pathog **17,** e1009957.

Brabham, H.J., Gómez De La Cruz, D., Were, V., Shimizu, M., Saitoh, H., Hernández-Pinzón, I., Green, P., Lorang, J., Fujisaki, K., Sato, K., Molnár, I., Šimková, H., Doležel, J., Russell, J., Taylor, J., Smoker, M., Gupta, Y.K., Wolpert, T., Talbot, N.J., Terauchi, R., and Moscou, M.J. (2023). Barley MLA3 recognizes the host-specificity effector Pwl2 from Magnaporthe oryzae. The Plant Cell**,** koad266.

Burnette, W.N. (1981). Burnette WN. "Western Blotting": electrophoretic transfer of proteins from sodium dodecyl sulfate-polyacrylamide gels to unmodified nitrocellulose and radiographic detection with antibody and radioiodinated protein. Analytical Biochemistry **112,** 195 - 203.

Cesari, S., Thilliez, G., Ribot, C., Chalvon, V., Michel, C., Jauneau, A., Rivas, S., Alaux, L., Kanzaki, H., Okuyama, Y., Morel, J.-B., Fournier, E., Tharreau, D., Terauchi, R., and Kroj, T. (2013). The Rice Resistance Protein Pair RGA4/RGA5 Recognizes the Magnaporthe oryzae Effectors AVR-Pia and AVR1-CO39 by Direct Binding The Plant Cell **25,** 1463-1481.

Cowan, G.H., Roberts, A.G., Jones, S., Kumar, P., Kalyandurg, P.B., Gil, J.F., Savenkov, E.I., Hemsley, P.A., and Torrance, L. (2018). Potato Mop-Top Virus Co-Opts the Stress Sensor HIPP26 for Long-Distance Movement. Plant Physiol **176,** 2052-2070.

Cruz, C.D., and Valent, B. (2017). Wheat blast disease: danger on the move. Trop Plant Pathol **42,** 210-222.

Cruz-Mireles, N., Eseola, A.B., Osés-Ruiz, M., Ryder, L.S., and Talbot, N.J. (2021). From appressorium to transpressorium—Defining the morphogenetic basis of host cell invasion by the rice blast fungus. PLOS Pathogens **17,** e1009779.

Cui, W., and Lee, J.-Y. (2016). Arabidopsis callose synthases CalS1/8 regulate plasmodesmal permeability during stress. Nature Plants **2,** 16034.

de Abreu-Neto, J.B., Turchetto-Zolet, A.C., de Oliveira, L.F.V., Bodanese Zanettini, M.H., and Margis-Pinheiro, M. (2013). Heavy metal-associated isoprenylated plant protein (HIPP): characterization of a family of proteins exclusive to plants. The FEBS Journal **280,** 1604-1616.

de Guillen, K., Ortiz-Vallejo, D., Gracy, J., Fournier, E., Kroj, T., and Padilla, A. (2015). Structure Analysis Uncovers a Highly Diverse but Structurally Conserved Effector Family in Phytopathogenic Fungi. PLoS Pathog **11,** e1005228.

Dean, R.A., Talbot, N.J., Ebbole, D.J., Farman, M.L., Mitchell, T.K., Orbach, M.J., Thon, M., Kulkarni, R., Xu, J.R., Pan, H., Read, N.D., Lee, Y.H., Carbone, I., Brown, D., Oh, Y.Y., Donofrio, N., Jeong, J.S., Soanes, D.M., Djonovic, S., Kolomiets, E., Rehmeyer, C., Li, W., Harding, M., Kim, S., Lebrun, M.H., Bohnert, H., Coughlan, S., Butler, J., Calvo, S., Ma, L.J., Nicol, R., Purcell, S., Nusbaum, C., Galagan, J.E., and Birren, B.W. (2005). The genome sequence of the rice blast fungus Magnaporthe grisea. Nature **434,** 980-986.

Dykema, P.E., Sipes, P.R., Marie, A., Biermann, B.J., Crowell, D.N., and Randall, S.K. (1999). A new class of proteins capable of binding transition metals. Plant Molecular Biology **41,** 139-150.

Foster, A.J., Martin-Urdiroz, M., Yan, X., Wright, H.S., Soanes, D.M., and Talbot, N.J. (2018). CRISPR-Cas9 ribonucleoprotein-mediated co-editing and counterselection in the rice blast fungus. Scientific Reports **8,** 14355.

Fukuoka, S., Saka, N., Koga, H., Ono, K., Shimizu, T., Ebana, K., Hayashi, N., Takahashi, A., Hirochika, H., Okuno, K., and Yano, M. (2009). Loss of function of a proline-containing protein confers durable disease resistance in rice. Science **325,** 998-1001.

Gao, W., Xiao, S., Li, H.-Y., Tsao, S.-W., and Chye, M.-L. (2009). Arabidopsis thaliana acyl-CoA-binding protein ACBP2 interacts with heavy-metal-binding farnesylated protein AtFP6. New Phytologist **181,** 89-102.

Giraldo, M.C., Dagdas, Y.F., Gupta, Y.K., Mentlak, T.A., Yi, M., Martinez-Rocha, A.L., Saitoh, H., Terauchi, R., Talbot, N.J., and Valent, B. (2013). Two distinct secretion systems facilitate tissue invasion by the rice blast fungus Magnaporthe oryzae. Nat Commun **4,** 1996.

Gómez De La Cruz, D., Zdrzałek, R., Banfield, M.J., Talbot, N.J., and Moscou, M.J. (2024). Molecular mimicry of a pathogen virulence target by a plant immune receptor. bioRxiv, 2024.2007.2026.605320.

Guo, T., Weber, H., Niemann, M.C.E., Theisl, L., Leonte, G., Novák, O., and Werner, T. (2021). Arabidopsis HIPP proteins regulate endoplasmic reticulum-associated degradation of CKX proteins and cytokinin responses. Mol Plant **14,** 1918-1934.

Hála, M., and Žárský, V. (2019). Protein Prenylation in Plant Stress Responses. In Molecules.

Hensel, G., Kastner, C., Oleszczuk, S., Riechen, J., and Kumlehn, J. (2009). Agrobacterium-mediated gene transfer to cereal crop plants: current protocols for barley, wheat, triticale, and maize. Int J Plant Genomics **2009,** 835608.

Holsters, M., Silva, B., Van Vliet, F., Genetello, C., De Block, M., Dhaese, P., Depicker, A., Inze, D., Engler, G., Villarroel, R., and et al. (1980). The functional organization of the nopaline A. tumefaciens plasmid pTiC58. Plasmid **3,** 212-230.

Imran, Q.M., Falak, N., Hussain, A., Mun, B.G., Sharma, A., Lee, S.U., Kim, K.M., and Yun, B.W. (2016). Nitric Oxide Responsive Heavy Metal-Associated Gene AtHMAD1 Contributes to Development and Disease Resistance in Arabidopsis thaliana. Front Plant Sci **7,** 1712.

Inoue, Y., Vy, T.T.P., Yoshida, K., Asano, H., Mitsuoka, C., Asuke, S., Anh, V.L., Cumagun, C.J.R., Chuma, I., Terauchi, R., Kato, K., Mitchell, T., Valent, B., Farman, M., and Tosa, Y. (2017). Evolution of the wheat blast fungus through functional losses in a host specificity determinant. Science **357,** 80-83.

Jones, J.D., and Dangl, J.L. (2006). The plant immune system. Nature **444,** 323-329.

Kang, S.C., Sweigard, J.A., and B, V. (1995). The PWL host specificity gene family in the blast fungus Magnaporthe grisea. Molecular Plant-Microbe Interactions **8,** 939-948.

Kankanala, P., Czymmek, K., and Valent, B. (2007). Roles for rice membrane dynamics and plasmodesmata during biotrophic invasion by the blast fungus. Plant Cell **19,** 706-724.

Kanzaki, H., Yoshida, K., Saitoh, H., Fujisaki, K., Hirabuchi, A., Alaux, L., Fournier, E., Tharreau, D., and Terauchi, R. (2012). Arms race co-evolution of Magnaporthe oryzae AVR-Pik and rice Pik genes driven by their physical interactions. The Plant Journal **72,** 894-907.

Khang, C.H., Berruyer, R., Giraldo, M.C., Kankanala, P., Park, S.-Y., Czymmek, K., Kang, S., and Valent, B. (2010). Translocation of Magnaporthe oryzae Effectors into Rice Cells and Their Subsequent Cell-to-Cell Movement The Plant Cell **22,** 1388-1403.

Li, H., and Durbin, R. (2009). Fast and accurate short read alignment with Burrows-Wheeler transform. Bioinformatics **25,** 1754-1760.

Li, H., Wang, J., Kuan, T.A., Tang, B., Feng, L., Wang, J., Cheng, Z., Skłenar, J., Derbyshire, P., Hulin, M., Li, Y., Zhai, Y., Hou, Y., Menke, F.L.H., Wang, Y., and Ma, W. (2023). Pathogen protein modularity enables elaborate mimicry of a host phosphatase. Cell **186,** 3196-3207.e3117.

Maidment, J.H.R., Franceschetti, M., Maqbool, A., Saitoh, H., Jantasuriyarat, C., Kamoun, S., Terauchi, R., and Banfield, M.J. (2021). Multiple variants of the fungal effector AVR-Pik bind the HMA domain of the rice protein OsHIPP19, providing a foundation to engineer plant defense. Journal of Biological Chemistry **296**.

Maqbool, A., Saitoh, H., Franceschetti, M., Stevenson, C.E.M., Uemura, A., Kanzaki, H., Kamoun, S., Terauchi, R., and Banfield, M.J. (2015). Structural basis of pathogen

914 recognition by an integrated HMA domain in a plant NLR immune receptor. eLife **4,**
915 e08709.

916 **Meng, E.C., Goddard, T.D., Pettersen, E.F., Couch, G.S., Pearson, Z.J., Morris, J.H., and**
917 **Ferrin, T.E.** (2023). UCSF ChimeraX: Tools for structure building and analysis.
918 Protein Sci **32,** e4792.

919 **Mosquera, G., Giraldo, M.C., Khang, C.H., Coughlan, S., and Valenta, B.** (2009).
920 Interaction Transcriptome Analysis Identifies Magnaporthe oryzae BAS1-4 as
921 Biotrophy-Associated Secreted Proteins in Rice Blast Disease. American Society of
922 Plant Biologists **21,** 1273–1290.

923 **Mukhi, N., Brown, H., Gorenkin, D., Ding, P., Bentham, A.R., Stevenson, C.E.M., Jones,**
924 **J.D.G., and Banfield, M.J.** (2021). Perception of structurally distinct effectors by the
925 integrated WRKY domain of a plant immune receptor. Proc Natl Acad Sci U S A **118**.

926 **Mutiga, S.K., Rotich, F., Were, V.M., Kimani, J.M., Mwongera, D.T., Mgonja, E., Onaga,**
927 **G., Konaté, K., Razanaboahirana, C., Bigirimana, J., Ndayiragije, A., Gichuhi, E.,**
928 **Yanoria, M.J., Otipa, M., Wasilwa, L., Ouedraogo, I., Mitchell, T., Wang, G.-L.,**
929 **Correll, J.C., and Talbot, N.J.** (2021). Integrated Strategies for Durable Rice Blast
930 Resistance in Sub-Saharan Africa. Plant Disease **105,** 2749-2770.

931 **O'Lexy, R., Kasai, K., Clark, N., Fujiwara, T., Sozzani, R., and Gallagher, K.L.** (2018).
932 Exposure to heavy metal stress triggers changes in plasmodesmatal permeability via
933 deposition and breakdown of callose. Journal of Experimental Botany **69,** 3715-3728.

934 **Oikawa, K., Fujisaki, K., Shimizu, M., Takeda, T., Nemoto, K., Saitoh, H., Hirabuchi, A.,**
935 **Hiraka, Y., Miyaji, N., Białas, A., Langner, T., Kellner, R., Bozkurt, T.O., Cesari,**
936 **S., Kroj, T., Banfield, M.J., Kamoun, S., and Terauchi, R.** (2024). The blast
937 pathogen effector AVR-Pik binds and stabilizes rice heavy metal-associated (HMA)
938 proteins to co-opt their function in immunity. PLOS Pathogens **20,** e1012647.

939 **Oliveira-Garcia, E., Yan, X., Oses-Ruiz, M., de Paula, S., and Talbot, N.J.** (2023a).
940 Effector-triggered susceptibility by the rice blast fungus Magnaporthe oryzae. New
941 Phytologist **n/a**.

942 **Oliveira-Garcia, E., Tamang, T.M., Park, J., Dalby, M., Martin-Urdiroz, M., Rodriguez**
943 **Herrero, C., Vu, A.H., Park, S., Talbot, N.J., and Valent, B.** (2023b). Clathrin-
944 mediated endocytosis facilitates the internalization of Magnaporthe oryzae effectors
945 into rice cells. The Plant Cell **35,** 2527-2551.

946 **Ortiz, D., de Guillen, K., Cesari, S., Chalvon, V., Gracy, J., Padilla, A., and Kroj, T.**
947 (2017). Recognition of the Magnaporthe oryzae Effector AVR-Pia by the Decoy
948 Domain of the Rice NLR Immune Receptor RGA5. The Plant Cell **29,** 156-168.

949 **Ou, S.H.** (1980). Pathogen Variability and Host-Resistance in Rice Blast Disease. Annu Rev
950 Phytopathol **18,** 167-187.

951 **Radakovic, Z.S., Anjam, M.S., Escobar, E., Chopra, D., Cabrera, J., Silva, A.C., Escobar,**
952 **C., Sobczak, M., Grundler, F.M.W., and Siddique, S.** (2018). Arabidopsis HIPP27
953 is a host susceptibility gene for the beet cyst nematode Heterodera schachtii. Mol Plant
954 Pathol **19,** 1917-1928.

Sakulkoo, W., Osés-Ruiz, M., Oliveira Garcia, E., Soanes, D.M., Littlejohn, G.R., Hacker, C., Correia, A., Valent, B., and Talbot, N.J. (2018). A single fungal MAP kinase controls plant cell-to-cell invasion by the rice blast fungus. Science **359,** 1399-1403.

Sugihara, Y., Abe, Y., Takagi, H., Abe, A., Shimizu, M., Ito, K., Kanzaki, E., Oikawa, K., Kourelis, J., Langner, T., Win, J., Białas, A., Lüdke, D., Contreras, M.P., Chuma, I., Saitoh, H., Kobayashi, M., Zheng, S., Tosa, Y., Banfield, M.J., Kamoun, S., Terauchi, R., and Fujisaki, K. (2023). Disentangling the complex gene interaction networks between rice and the blast fungus identifies a new pathogen effector. PLOS Biology **21,** e3001945.

Suzuki, N., Yamaguchi, Y., Koizumi, N., and Sano, H. (2002). Functional characterization of a heavy metal binding protein CdI19 from Arabidopsis. The Plant Journal **32,** 165-173.

Sweigard, J.A., Carroll, A.M., Kang, S., Farrall, L., Chumley, F.G., and Valent, B. (1995). Identification, cloning, and characterization of PWL2, a gene for host species specificity in the rice blast fungus. Plant Cell **7,** 1221-1233.

Talbot, N.J. (2003). On the trail of a cereal killer: Exploring the biology of Magnaporthe grisea. Annu Rev Microbiol **57,** 177-202.

Talbot, N.J., Ebbole, D.J., and Hamer, J.E. (1993). Identification and characterization of MPG1, a gene involved in pathogenicity from the rice blast fungus Magnaporthe grisea. Plant Cell **5,** 1575-1590.

Valent, B., Farrall, L., and Chumley, F.G. (1991). Magnaporthe-Grisea Genes for Pathogenicity and Virulence Identified through a Series of Backcrosses. Genetics **127,** 87-101.

Wang, Z., Zhang, H., Li, Y., Chen, Y., Tang, X., Zhao, J., Yu, F., Wang, H., Xiao, J., Liu, J., Zhang, X., Sun, L., Xie, Q., and Wang, X. (2023). Isoprenylation modification is required for HIPP1-mediated powdery mildew resistance in wheat. Plant Cell Environ **46,** 288-305.

Were, V., and Talbot, N.J. (2023). Breaking the biotrophic interfacial complex: How genome editing can lead to rice blast resistance. Molecular Plant **16,** 1243-1245.

Wilson, R.A., and Talbot, N.J. (2009). Under pressure: investigating the biology of plant infection by Magnaporthe oryzae. Nat Rev Microbiol **7,** 185-195.

Yan, X., Tang, B., Ryder, L.S., MacLean, D., Were, V.M., Eseola, A.B., Cruz-Mireles, N., Ma, W., Foster, A.J., Osés-Ruiz, M., and Talbot, N.J. (2023). The transcriptional landscape of plant infection by the rice blast fungus Magnaporthe oryzae reveals distinct families of temporally co-regulated and structurally conserved effectors. The Plant Cell **35,** 1360-1385.

Yu, D., Fan, R., Zhang, L., Xue, P., Liao, L., Hu, M., Cheng, Y., Li, J., Qi, T., Jing, S., Wang, Q., Bhatt, A., and Shen, Q.-H. (2023). HvWRKY2 acts as an immunity suppressor and targets HvCEBiP to regulate powdery mildew resistance in barley. The Crop Journal **11,** 99-107.

Yuen, E.L.H., Tumtas, Y., King, F., Ibrahim, T., Chan, L.I., Evangelisti, E., Tulin, F., Skłenar, J., Menke, F.L.H., Kamoun, S., Bubeck, D., Schornack, S., and Bozkurt, T.O. (2024). A pathogen effector co-opts a host RabGAP protein to remodel pathogen interface and subvert defense-related secretion. Science Advances **10,** eado9516.

Zdrzałek, R., Xi, Y., Langner, T., Bentham, A.R., Petit-Houdenot, Y., De la Concepcion, J.C., Harant, A., Shimizu, M., Were, V., Talbot, N.J., Terauchi, R., Kamoun, S., and Banfield, M.J. (2024). Bioengineering a plant NLR immune receptor with a robust binding interface toward a conserved fungal pathogen effector. Proceedings of the National Academy of Sciences **121,** e2402872121.

Zhang, H., Zhang, X., Liu, J., Niu, Y., Chen, Y., Hao, Y., Zhao, J., Sun, L., Wang, H., Xiao, J., and Wang, X. (2020). Characterization of the Heavy-Metal-Associated Isoprenylated Plant Protein (HIPP) Gene Family from Triticeae Species. Int J Mol Sci **21**.

Zhang, S., and Xu, J.R. (2014). Effectors and effector delivery in Magnaporthe oryzae. PLoS Pathog **10,** e1003826.

Zhang, X., He, D., Zhao, Y., Cheng, X., Zhao, W., Taylor, I.A., Yang, J., Liu, J., and Peng, Y.-L. (2018). A positive-charged patch and stabilized hydrophobic core are essential for avirulence function of AvrPib in the rice blast fungus. The Plant Journal **96,** 133-146.

Zschiesche, W., Barth, O., Daniel, K., Böhme, S., Rausche, J., and Humbeck, K. (2015). The zinc-binding nuclear protein HIPP3 acts as an upstream regulator of the salicylate-dependent plant immunity pathway and of flowering time in Arabidopsis thaliana. New Phytologist **207,** 1084-1096.

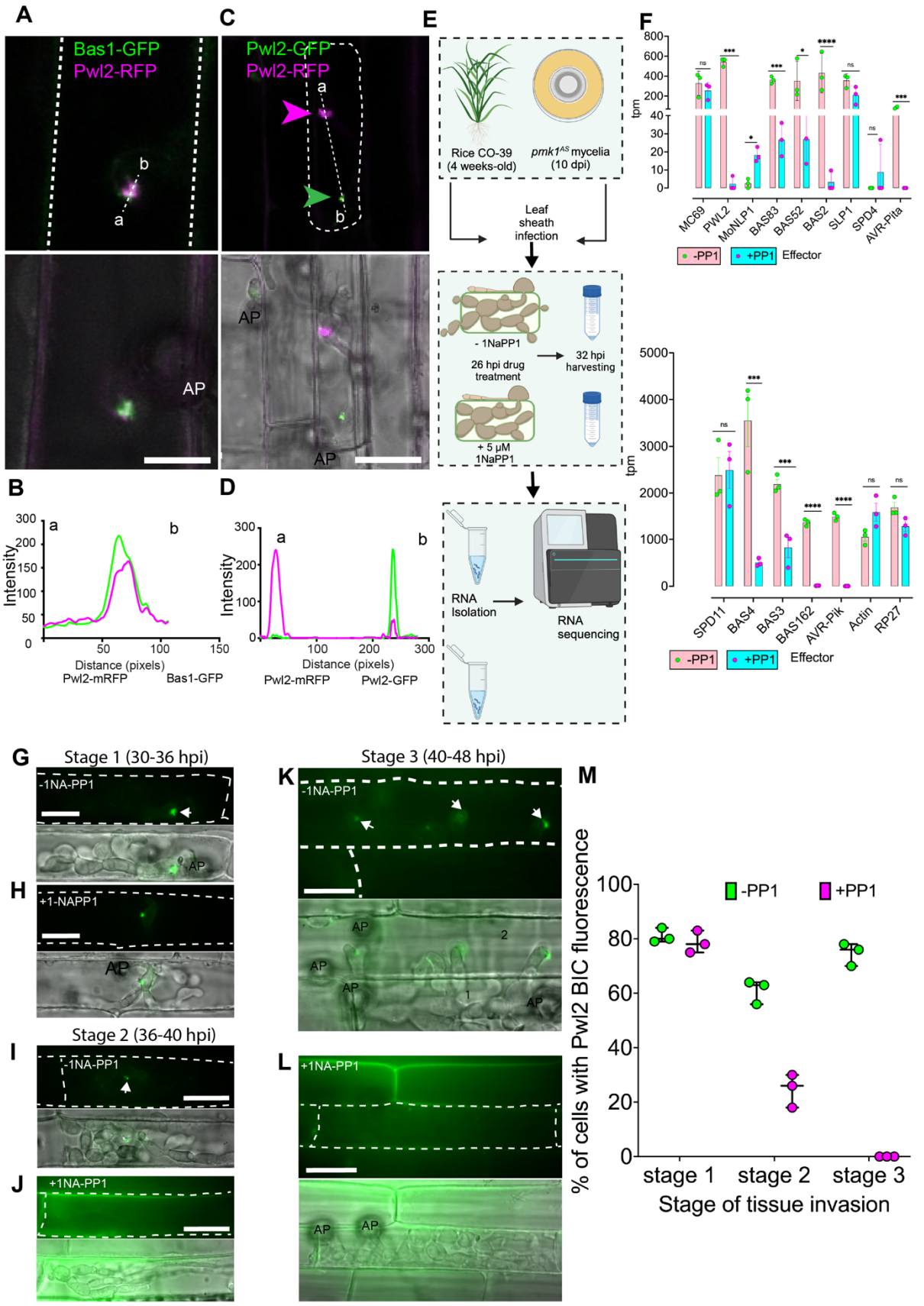

Fig.1. *PWL2* expression is regulated in a Pmk1-dependent manner during host infection. (**A+B**) Micrographs and line scan graph showing Pwl2 secreted through the Biotrophic Interfacial Complex (BIC) in rice cells during early infection. Conidial suspension at 1x 10^5

1023 mL^{-1} of *M. oryzae* strain co-expressing two BIC localised effectors, Bas1-GFP and Pwl2-mRFP
1024 were inoculated onto a susceptible cultivar Moukoto rice leaf sheath and images captured at 26
1025 hpi. Fluorescence of the two effectors was observed as small punctate signals in the same BIC.
1026 (**C+D**) Co-infection assay of rice leaf sheath with two different *M. oryzae* strains, one
1027 expressing Pwl2-mRFP and the other Pwl2-GFP at 30 hours post-infection (hpi). Micrographs
1028 and line scan graph shows there is an absence of mixed fluorescence confirming the BIC does
1029 not contain Pwl2 transferred from rice cells. BICs indicated by magenta arrows for mRFP and
1030 green arrows for GFP. (**E**) Schematic illustration to describe the workflow used to test genes
1031 regulated in a Pmk1-dependent manner. Rice leaf sheaths were infected with a *M. oryzae*
1032 *pmk1^{AS}* mutant spores before mock or 1NA-PP1 treatment. Treated and mock treated, infected
1033 leaf sheaths were trimmed and used for RNA isolation followed by sequencing. Figure created
1034 with BioRender https://biorender.com/. (**F**) Bar charts to show that a subset of effectors is
1035 regulated in a manner that requires Pmk1. Gene expression is shown as TPM (transcripts per
1036 million) at 32 hpi. (**G-L**) Micrographs showing expression of Pwl2-GFP by *M. oryzae pmk1^{AS}*
1037 in leaf sheaths of a susceptible rice line CO39 using conidial suspension at 1x 10^5 mL^{-1}.
1038 Fluorescence of Pwl2 at different stages of infectious hyphal progression, starting with early
1039 stage of infection, Stage 1 (30-36 hpi) where a newly differentiated bulbous hyphae is formed
1040 as per (Sakulkoo *et al.*, 2018). Analysis was also carried out at later stages of infection
1041 including Stage 2 (36-40 hpi) where a primary invaded cell is filled with differentiated bulbous
1042 hyphae) and Stage 3 (40-48 hpi) where colonization of primary invaded cell is complete and
1043 there is full invasion of secondary invaded cells. To test Pmk1 inhibition, inoculated leaf
1044 sheaths were treated with 5 µM 1NA-PP1 at 26 hpi. (**M**) Inhibition of Pwl2 by 1NA-PP1 is
1045 quantified as percentage of cells showing Pwl2 fluorescence in the BIC. Arrows indicate
1046 fluorescence in the BIC. Scale bars represent 20 µm. The primary and secondary invaded cells
1047 are indicated with 1 and 2 respectively. Significance between groups of samples was performed
1048 using Unpaired Student's t-test. ****$P<0.0001$, **$P<0.01$, *$P<0.05$, NS indicates no
1049 significant difference.
1050
1051

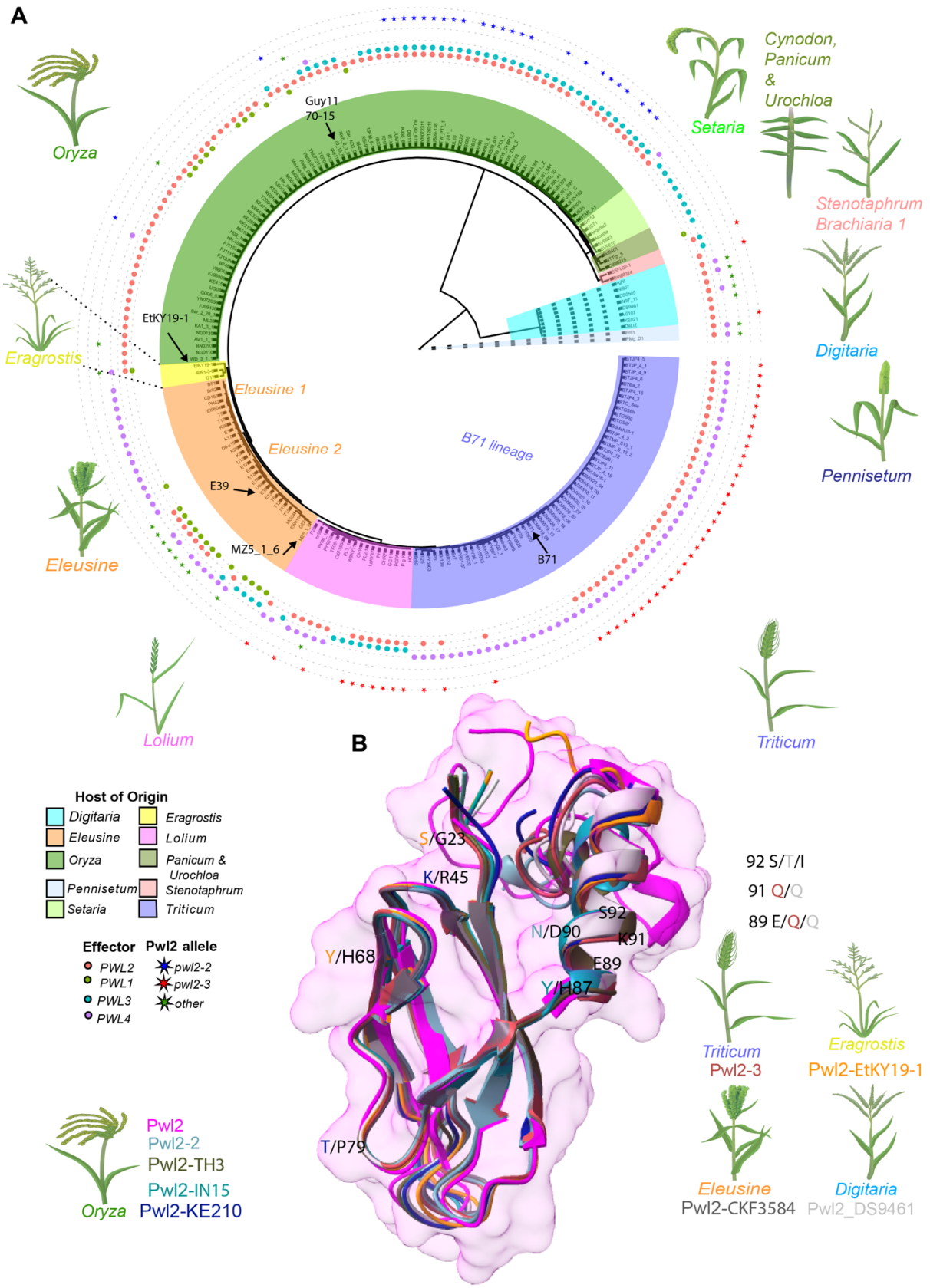

Fig. 2. **Pwl2 is highly conserved in isolates of *M. oryzae* and displays conserved structural features.**

1055 (**A)** Phylogenetic analysis and *PWL* gene family distribution in *M. oryzae*. A maximum
1056 parsimony tree was generated using kSNP3 to include isolates from different host-limited
1057 forms of *M. oryzae* including isolates that infect *Oryza sativa* (rice), *Eleusine* spp. (finger
1058 millet), *Hordeum vulgare* (barley), *Setaria* spp. (foxtail millet), *Triticum aestivum* (wheat),
1059 *Lolium* spp. (rye grass), *Brachiaria* spp. (signal grass), *Panicum* spp. (torpedo grass),
1060 *Eragrostis* spp. (weeping lovegrass), *Stenotaphrum* spp. (buffalo grass), *Cynodon* spp.
1061 (Bermuda grass) and *Urochloa* spp. (signal grass) (Ou, 1980; Talbot, 2003; Cruz and Valent,
1062 2017; Inoue *et al.*, 2017), as well as *Magnaporthe* species that infect *Digitaria sanguinalis*
1063 (crabgrass) and *Pennisetum* spp. (pearl millet). We used Pwl1 (BAH22184.1), Pwl2
1064 (QNS36448.1), Pwl3 (AAA80240.1) and Pwl4 (AAA80241.1) protein sequences to query the
1065 presence or absence of each gene using tblastn. The heatmap indicates the presence/absence of
1066 genes in the *PWL* family. *PWL1* is predominantly present in group EC-1I (Asuke *et al.*, 2020)
1067 of *Eleusine*-infecting isolates and some *Oryza*-infecting isolates, but largely absent from other
1068 host-specific lineages, except one *Eragrostis*-infecting isolate, EtK19-1, and one *Cynodon*-
1069 infecting isolate, Cd88215, but not in *Digitaria* and *Pennisetum* spp lineages. *PWL3* is present
1070 in most *Oryza*-infecting isolates, some *Setaria*, *Lolium*, and *Eleusine*-infecting isolates but
1071 largely absent in *Eragrostis* and *Triticum* lineages, as well as *Digitaria* and *Pennisetum*
1072 lineages. *PWL4* is present in *Eleusine*, *Eragrostis, Lolium* and *Triticum*-infecting isolates, but
1073 only two *Oryza*-infecting isolates. Several *Pennisetum* and *Digitaria*-infecting isolates,
1074 however, carry *PWL4. PWL2* is found in most host-limited forms of *M. oryzae* and related
1075 *Magnaporthe* species but absent in *Brachiaria, Setaria, Panicum, Cynodon* and *Urochloa*. (**B**)
1076 Superimposition of different Pwl2 variants predicted using AlphaFold3 onto the resolved Pwl2
1077 structure (magenta) indicating region of polymorphism. Different color represent different
1078 variant as follows, Pwl2-2 (teal), Pwl2-3 (brick red), Pwl2-TH3 (dark olive green), Pwl2-IN15
1079 (dark teal), Pwl2-KE210 (blue), Pwl2-CKF3584 (dark grey), Pwl2-EtKY19-1 (orange), Pwl2-
1080 DS9461 (light grey). The superimposition shows overall structural conservation in MAX-fold,
1081 without the signal peptide and the C-terminus. The variants of Pwl2 are named with
1082 corresponding isolate name and grouped according to host species. Varying residues are
1083 colored according to the genome from which they were identified.
1084

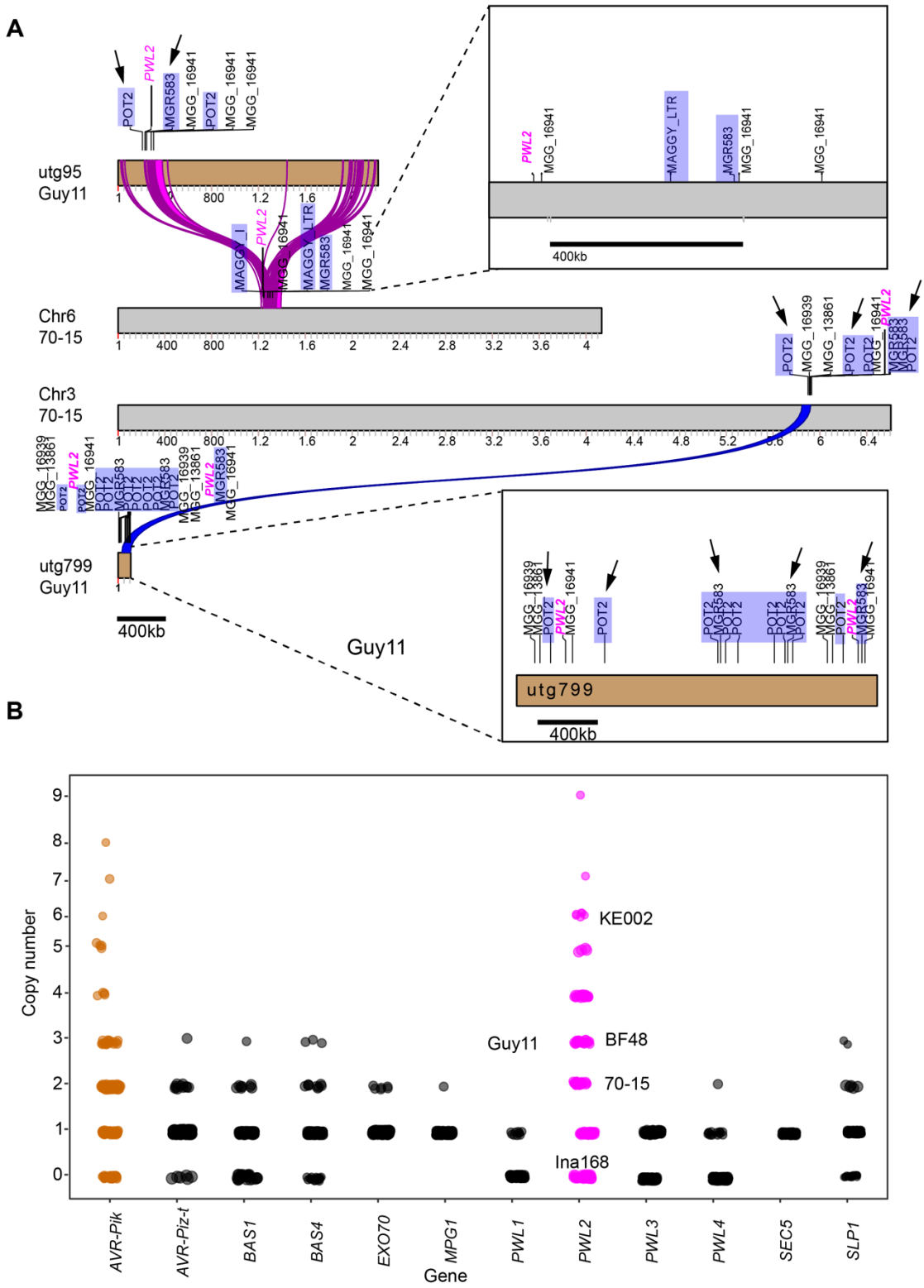

Fig. 3. *PWL2* has undergone copy number expansion in *M. oryzae* field isolates. **(A)** Schematic diagram showing the estimated chromosomal location of *PWL2* on multiple loci (Chr3 and 6) of the reference genome 70-15 and on equivalent region of assembled contigs of laboratory strain Guy11 genome. *PWL2* is flanked by *POT2* and *MGR583* repeated sequences suggesting a possible involvement in translocation of events into different loci in the genome.

1091 Arrows indicate location of *POT2* and *MGR58* while *PWL2* is labelled in magenta. (**B)** A k-
1092 mer analysis on sequenced raw reads was used to determine copy number variation of *PWL*
1093 family genes in different *M. oryzae* isolates. Plot shows high copy number of *PWL2* in analyzed
1094 genomes (n = 286) compared to the other *PWL* gene family members, another effector *SLP1,*
1095 and selected control genes *MPG1* and *SEC5*. Similarly, *AVR-Pik* shows multiple copies in
1096 different isolates. Copy number of *PWL2* in selected isolates Guy11, KE002, BF48, 70-15 is
1097 indicated with Ina168 that lack *PWL2* used as a negative control.
1098
1099

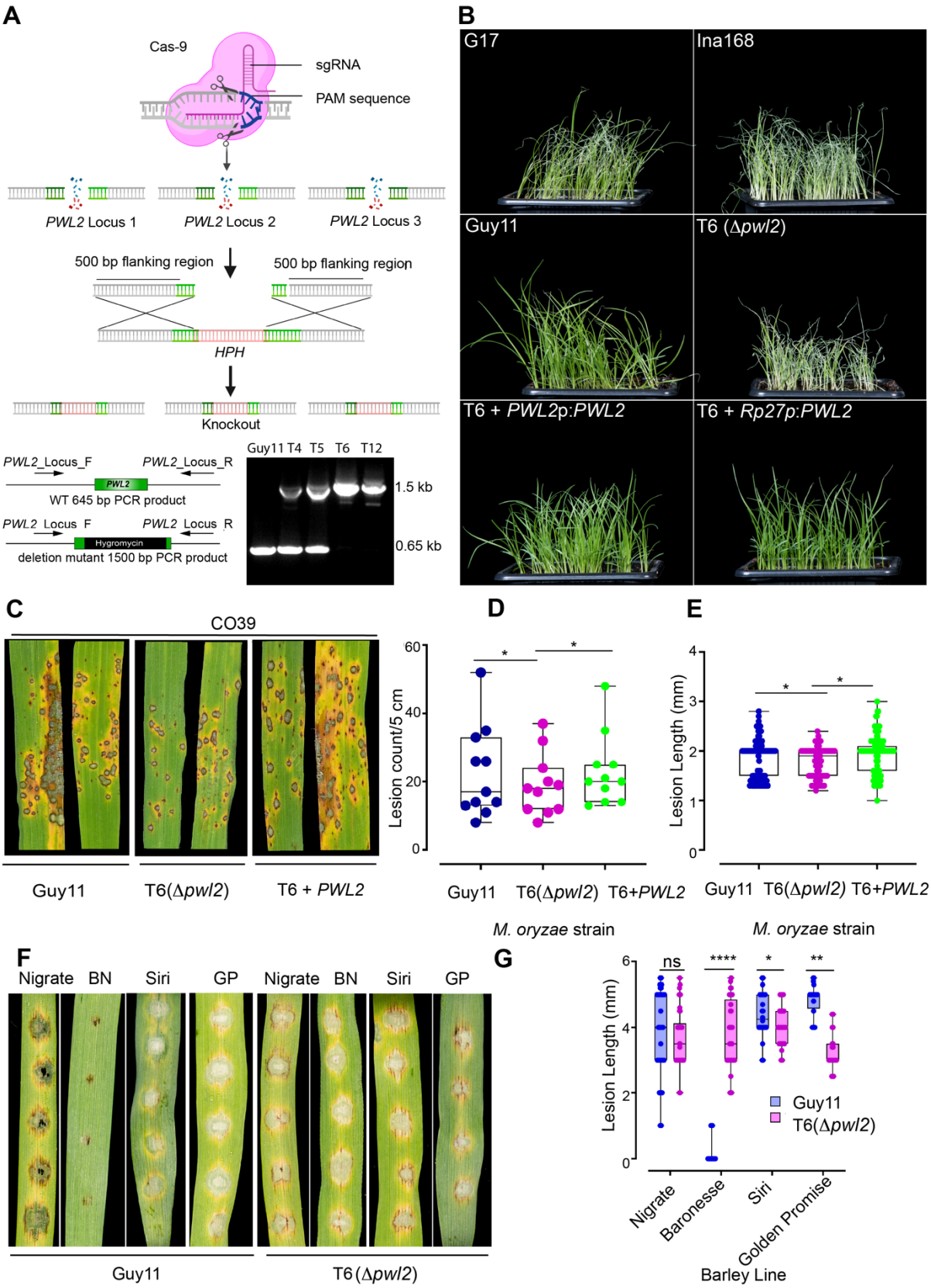

1100

1101 **Fig. 4. CRISPR-Cas9 *Δpwl2* mutants demonstrate Pwl2 as both host range and a**

1102 **virulence factor**

1103 **(A)** Schematic illustration of the CRISPR-Cas9 mediated gene editing process for inserting the
1104 Hygromycin Phosphotransferase (*HPH*) gene cassette at the *PWL2* locus. The guided sequence
1105 (sgPWL2) directs Cas9 to introduce a double stranded break at the *PWL2* locus, with the DNA
1106 repair template containing the Hygromycin resistance gene cassette and flanking regions of the
1107 *PWL2* gene. This leads to mutations in the form of indels or gene replacements. Figure created
1108 with BioRender https://biorender.com/. Positive mutants were identified by amplifying the
1109 hygromycin cassette from transformants with the three copies deleted. (**B)** Comparison of
1110 disease symptoms in weeping lovegrass (*E. curvula*) infected with different *M. oryzae* isolates.
1111 In the top panel, typical disease lesions produced by *E. curvula*-infecting isolate G17 (-*PWL2*)
1112 and a rice infecting isolate Ina168 (-*PWL2*) are shown. In the middle panel, CRISPR-Cas9
1113 deletion mutants exhibit gain of virulence on weeping lovegrass compared to Guy11. In the
1114 bottom panel, complemented strains with both native and constitutive RP27 promotors showed
1115 a loss of virulence on weeping lovegrass. (**C**) *Δpwl2* mutants display reduced pathogenicity on
1116 rice cultivar CO39. Conidial suspensions from Guy11, *Δpwl2* (T6) and complemented
1117 *Δpwl2*(T6) +*PWL2*p:*PWL2*) were used to inoculate 21-day-old seedlings of the blast-
1118 susceptible cultivar CO39, and disease symptoms recorded after 5 dpi. The box plots show the
1119 lesion density (**D**) and lesion size (**E**) of seedlings infected with Guy11, *Δpwl2* (T6) and
1120 complemented *Δpwl2* (T6 +*PWL2*p:*PWL2*). (**F**) The *Δpwl2* mutant exhibits enhanced
1121 pathogenicity on barley cultivar Baronesse (*Mla3*). Conidial suspensions from Guy11 and
1122 *Δpwl2* T6 were used to inoculate 10-day old seedlings of barley lines Golden Promise, Siri,
1123 Nigrate and Baronesse, and disease symptoms recorded after 5 dpi. Conidial suspensions at 1
1124 $\times 10^5$ mL^{-1} spores/mL was used for infection assays. **(G)** The box plot shows lesion size of
1125 barley seedlings infected with Guy11 and *Δpwl2* (T6). The lower horizontal line shows the
1126 minimum value, and the upper horizontal line shows the maximum value. The lower border
1127 and upper border of the box shows the lower quartile and upper quartile, respectively. The line
1128 in the box shows the median. Significance between groups of samples was performed using
1129 Unpaired Student's t-test. ****$P<0.0001$, **$P<0.01$, *$P<0.05$, NS indicates no significant
1130 difference.

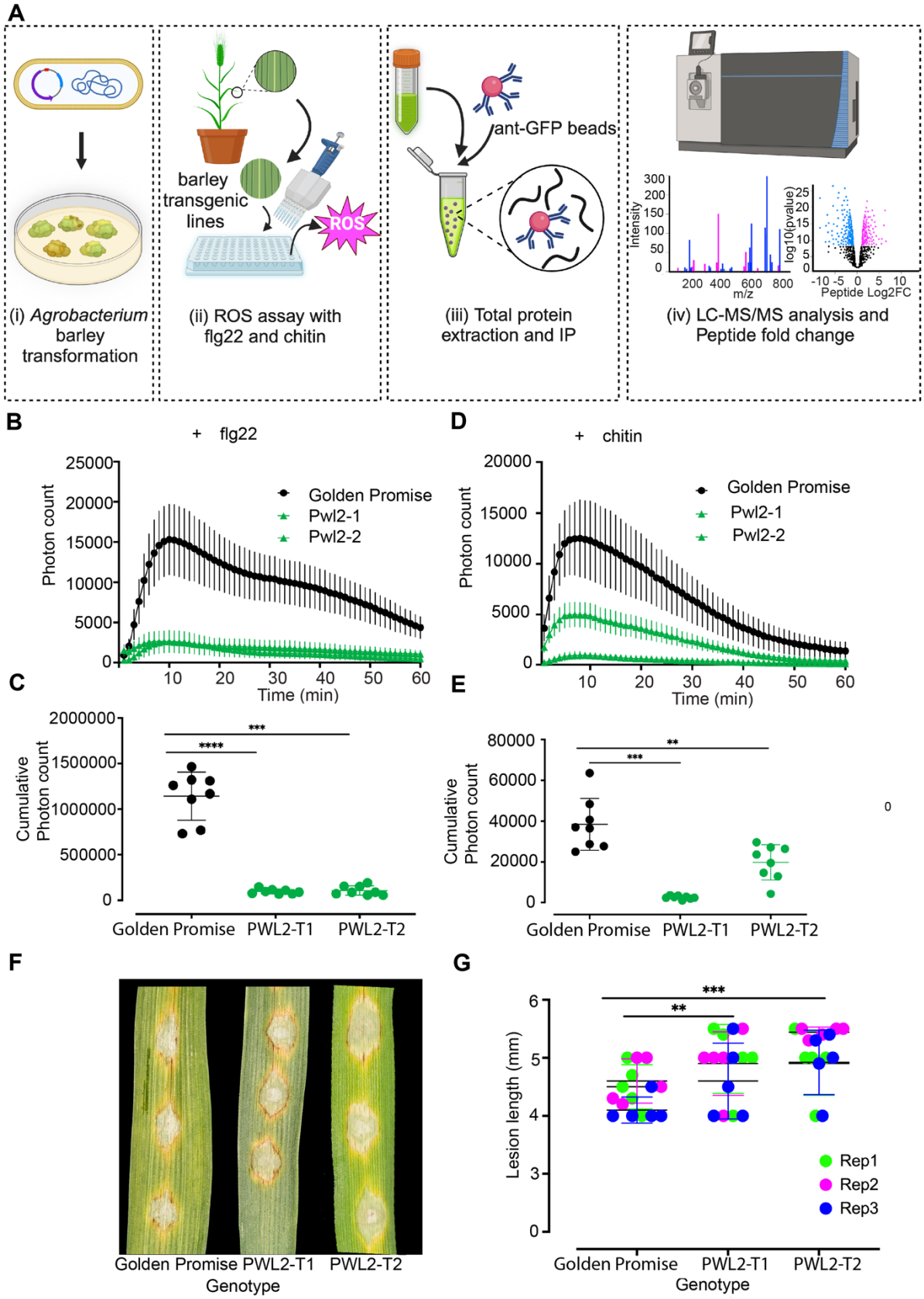

Fig. 5. Pwl2 suppresses PAMP-induced ROS in transgenic barley lines

1133 (**A**) Schematic illustration to describe the workflow used to generate transgenic plants, test for
1134 PTI response and identify putative Pwl2 interactors using discovery proteomics. ROS
1135 production in leaf discs collected from 4–week-old stable transgenic lines expressing Pwl2-
1136 YFP compared to cv. Golden Promise induced by 1 uM flg22 (**B-C**) or chitin (**D-E**) (n > 8).
1137 Points represent mean; error bars represent SEM. For ROS assay, line graphs (**B+D**) points
1138 represent mean per time point and dot plots represent cumulative ROS (**C+E**) production over
1139 60 min, error bars represent SEM. For dot plot, graphs show the average cumulative photon
1140 count for cv. Golden Promise control and two independent Pwl2-YFP lines. The lower
1141 horizontal line shows the minimum value, and the upper horizontal line shows the maximum
1142 value, the middle line shows the mean value. (**F)** Leaf drop infection on two independent barley
1143 transgenic lines expressing Pwl2-YFP compared to infection on wild type cv. Golden Promise
1144 3-4 dpi. (**G**) The dot plot represents the disease lesion length on cv. Golden Promise compared
1145 to two independent Pwl2-YFP transgenic lines. Unpaired Student's t-test was performed to
1146 determine significant differences ****P<0.0001, ***P<0.001, **P<0.01. These experiments
1147 were repeated three times to obtain consistent result.
1148
1149

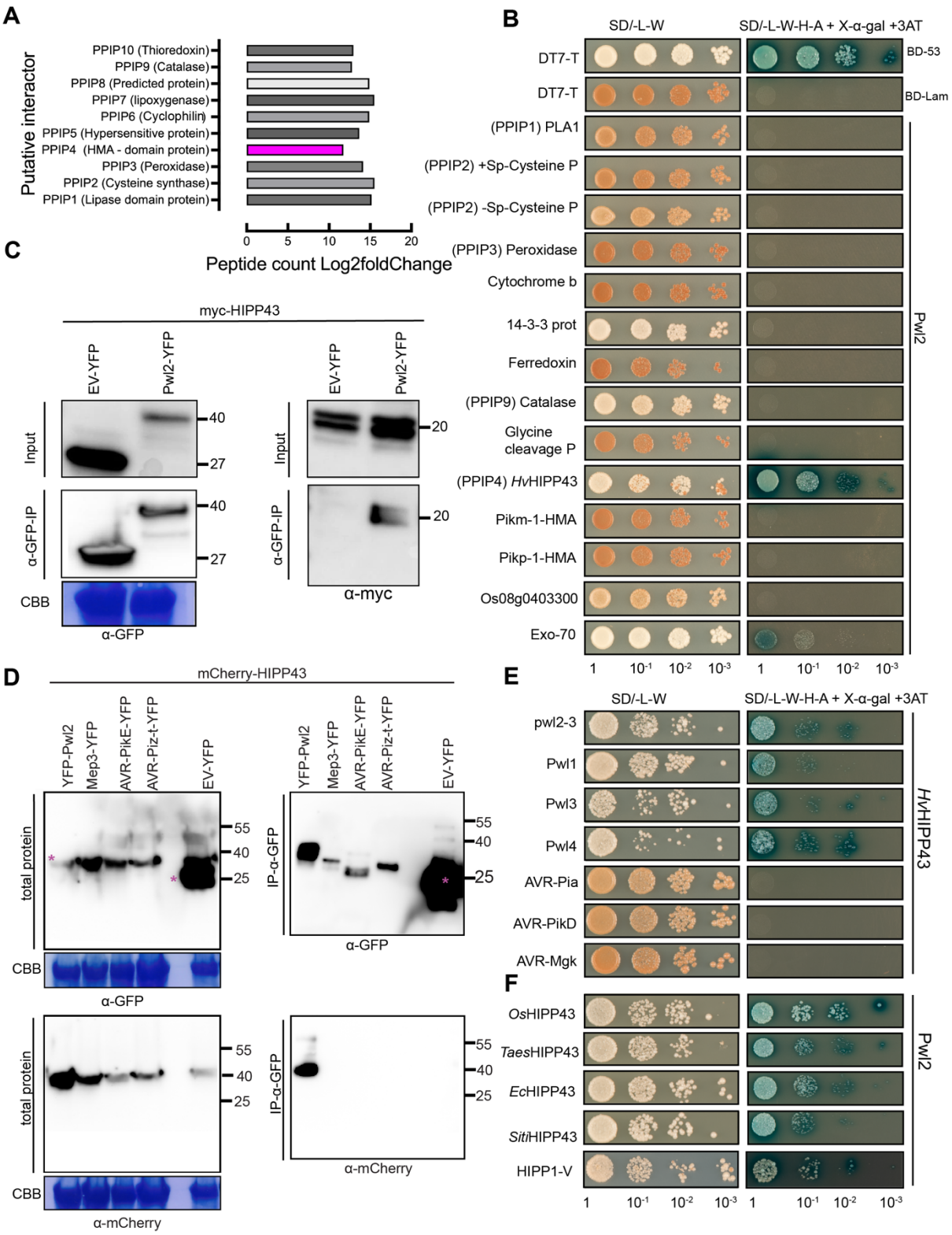

Fig. 6. Pwl2 interacts with HIPP43 and its orthologs from other grass species.

1152 (**A**) Putative Pwl2 interacting peptides were immunoprecipitated from protein extracts of 3-
1153 week-old stable cv. Golden Promise transgenic lines expressing Pwl2-YFP or free cytoplasmic
1154 YFP using anti-GFP antibodies, and LC-MS/MS was performed to identify unique putatively
1155 interacting peptides. The scale 0-20 represents the Log2fold change in peptides when compared
1156 to the control. (**B**) One-to-one yeast two-hybrid between Pwl2 and selected top candidates from
1157 IP-MS analysis, Pwl2 and Putative Pwl2 Interacting Proteins (PPIPs). HMA integrated in rice
1158 NLR Pikm-1 and Pikp-1 were used as specificity controls. Simultaneous co-transformation of
1159 pGADT7-Pwl2 (prey vector) and pGBK-PPIPs (bait vector) and PGBKT7-53 and pGADT7-T
1160 (positive control) pGADTT7-T and pGBKT7-Lam (negative control) into Y2H gold strain.
1161 Positive interaction resulted in the activation of four reporter genes and growth on high-
1162 stringency medium (−Ade, −Leu, –Trp, _His +X-α-gal and 3-amino-1,2,4-triazole). Co-
1163 transformation also activates the expression of *MEL1*, which results in the secretion of α–
1164 galactosidase and the hydrolysis of X-α-gal in the medium, turning the yeast colonies blue.
1165 HIPP43 exclusively interacts with Pwl2 in SD/-L-W-H-A X-α-gal medium with 3AT added.
1166 These experiments were repeated several times over three years obtaining consistent result. **(C)**
1167 Co-immunoprecipitation (co-IP) of Pwl2-YFP and Myc-HIPP43 or (**D**) mCherry-HIPP43 in
1168 *N. benthamiana* leaves. C-or N-terminal GFP tagged Pwl2 and C-terminal Myc-HIPP43 was
1169 cloned into the vector pGW514 and transformed into *Agrobacterium* strain *GV3101* and co-
1170 infiltrated into *N. benthamiana* leaves and left to incubate for 48 h. Immunoprecipitates were
1171 obtained with anti-GFP affinity matrix beads and probed with anti-GFP-peroxidase, anti-
1172 mCherry-peroxidase and anti-Myc-peroxidase (HRP-conjugated) antibodies. Total protein
1173 extracts were also probed with appropriate (HRP-conjugated) antibodies. (**E**) Yeast-two-hybrid
1174 analysis shows; upper panel, *Hv*HIPP43 interacts with *PWL* gene family products Pwl1, Pwl3,
1175 Pwl4 and variant *pwl2-3*. (**F**) Pwl2 interacts with HIPP43 homologs from rice (*Os*HIPP43),
1176 wheat (*Taes*HIPP43), weeping love grass (*Ec*HIPP43), foxtail millet (*SitiHIPP43*) and wild
1177 wheat (HIPP1-V). These experiments were repeated several times over three years obtaining
1178 consistent result.
1179

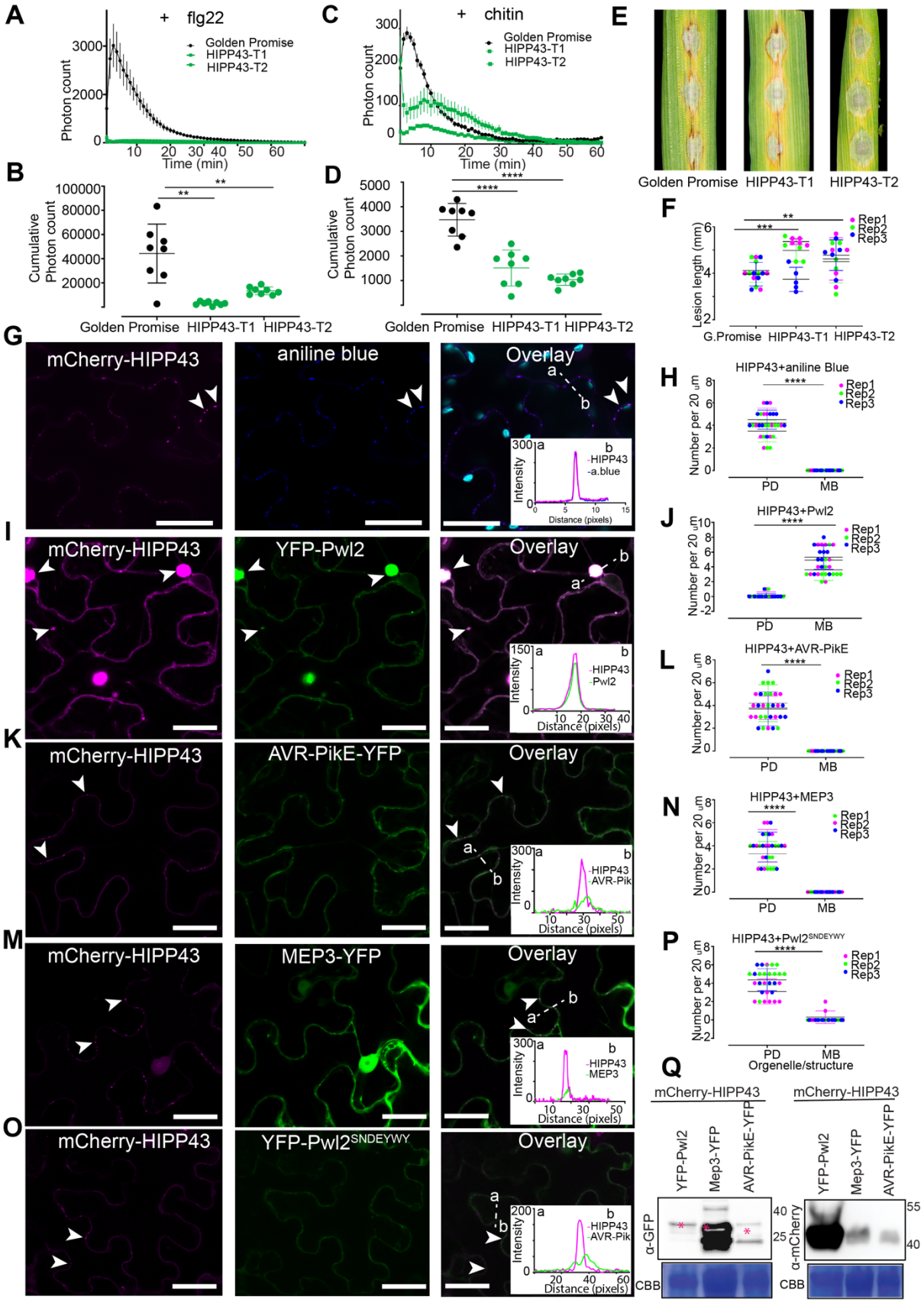

Fig. 7. *Hv*HIPP43 suppresses PAMP-induced ROS in transgenic barley and is stabilized by Pwl2.

1183 **(A-D)** ROS production measured from leaf disks collected from 4–week-old stable transgenic
1184 line expressing YFP-HIPP43 and cv. Golden promise (control) in the absence and presence of
1185 1 uM flg22 or 1 mg/ml Chitin (n > 8). For ROS assay, line graphs (**A+C**) points represent mean
1186 per time point and dot plots represent cumulative ROS (**B+D**) production over 60 min, error
1187 bars represent SEM for cv. Golden Promise control and two independent YFP-HIPP43 lines.
1188 For dot plot, graphs show the average cumulative photon count for cv. Golden Promise control
1189 and two independent YFP-HIPP43 lines. (**E**) Leaf drop infection on barley transgenic lines
1190 expressing YFP-HIPP43 compared to wild type Golden Promise. Conidial suspensions at 1
1191 $\times 10^5$ mL^{-1} spores/mL from Guy11 were used for inoculation. Disease symptoms were recorded
1192 after 4 dpi. (**F**) Dot plot showing lesion length on barley lines infected with Guy11. All
1193 experiments were repeated three times giving consistent results. **(G+H)** Micrographs and line
1194 scan graph showing mCherry-HIPP43 localizing as small puncta on the plasma membrane
1195 when expressed in *N. benthamiana.* Staining of callose using aniline blue overlaps with
1196 mCherry-HIPP43, confirming mCherry-HIPP43 localises exclusively at the plasmodesmata
1197 (PD) localization and cytoplasmic mobile bodies (MB) localization is absent. **(I+J)**
1198 Micrographs and line scan graph showing the presence of YFP-Pwl2, alters mCherry-HIPP43
1199 localisation, which was observed to translocate to the cytoplasm, mobile cytoplasmic bodies.
1200 **(K+L)** Micrographs and line scan graph showing mCherry-HIPP43 remains in the PD in the
1201 presence of cytoplasmically localised AVR-PikE**.** **(M+N**) Micrographs and line scan graph
1202 showing mCherry-HIPP43 remains in the PD in the presence of cytoplasmically and PD
1203 localised MEP3**.** (**O+P**) Micrographs and line scan graph showing mCherry-HIPP43 remains
1204 in the PD in the presence of $Pwl2^{SNDEYWY}$, a mutant that does not interact with HIPP43**.** Dotted
1205 lines in the overlay panels correspond to distance and direction of line intensity plot. Scale bars
1206 represent 20 µm**.** For dot plots, the lower horizontal line shows the minimum value, the upper
1207 horizontal line shows the maximum value, the middle line shows the mean value. Unpaired
1208 Student's t-test was performed to determine significant differences ****P<0.0001,
1209 ***P<0.001, **P<0.01. (**Q**) Western blot to show that Pwl2 does not degrade HIPP43. Total
1210 protein extracts from *N. benthamiana* leaves co-infiltrated with YFP-Pwl2, MEP3 or AVR-
1211 PikE and mCherry-HIPP43 were immunoblotted and probed with anti-GFP-peroxidase (left)
1212 or anti-mCherry-peroxidase (right) (HRP-conjugated) antibodies. Microscope imaging
1213 experiments were repeated several times over two years giving consistent result.

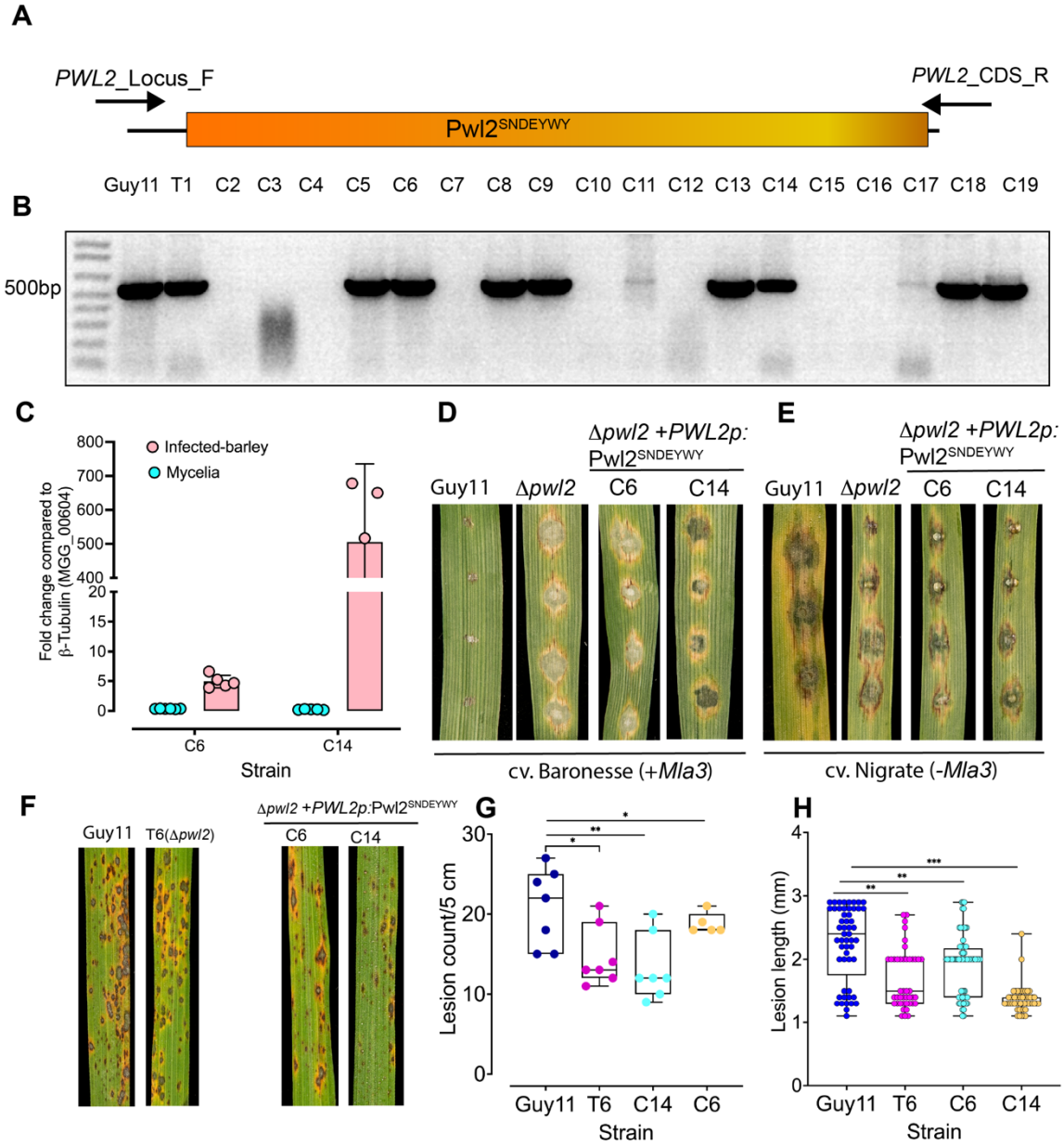

Fig. 8. Pwl2^{SNDEYWY} does not complement Mla3 recognition and virulence on a blast-susceptible rice cultivar CO39.

(**A and B**) Complemented *Δpwl2+PWL2*p:*Pwl2^{SNDEYWY}*) positive transformants were screened using PCR to amplify *PWL2* coding sequence. (**C**) Bar charts showing relative expression as log2 fold change of *Pwl2^{SNDEYWY}* in two selected transformants, C6 and C14 using qRT-PCR. Detached leaves of 10-day old seedlings of barley were inoculated with *Δpwl2+PWL2*p:*Pwl2^{SNDEYWY}*) and infected tissue collected 40 hpi and used for RNA isolation (3 biological replicates), cDNA synthesised and samples used for qRT-PCR. (**D and E**) *Δpwl2+PWL2*p:*Pwl2^{SNDEYWY}* complemented strains C6 and C14 produced compatible disease lesions on barley cultivar Baronesse (+*Mla3*) (**D**) and Nigrate (-*Mla3*) (**E**). Conidial

suspensions at 1 $\times 10^5$ mL^{-1} spores/mL from Guy11, *Δpwl2* and complemented *Δpwl2+PWL2*p:*Pwl2*^{SNDEYWY} were used to inoculate 10-day old seedlings of barley and disease symptoms recorded after 5 dpi. (**F-H**) Complemented *Δpwl2+PWL2*p:*Pwl2*^{SNDEYWY} display reduced pathogenicity on rice cultivar CO39. Conidial suspensions at 1 $\times 10^5$ mL^{-1} spores/mL from Guy11, *Δpwl2* T6 and complemented *Δpwl2+PWL2*p:*Pwl2*^{SNDEYWY} were used to inoculate 21-day-old seedlings of the blast-susceptible cultivar CO39, and disease symptoms recorded after 5 dpi. Significance between groups of samples was performed using Unpaired Student's t-test. ***$P<0.0001$, **$P<0.01$, *$P<0.05$, NS indicates no significant difference.

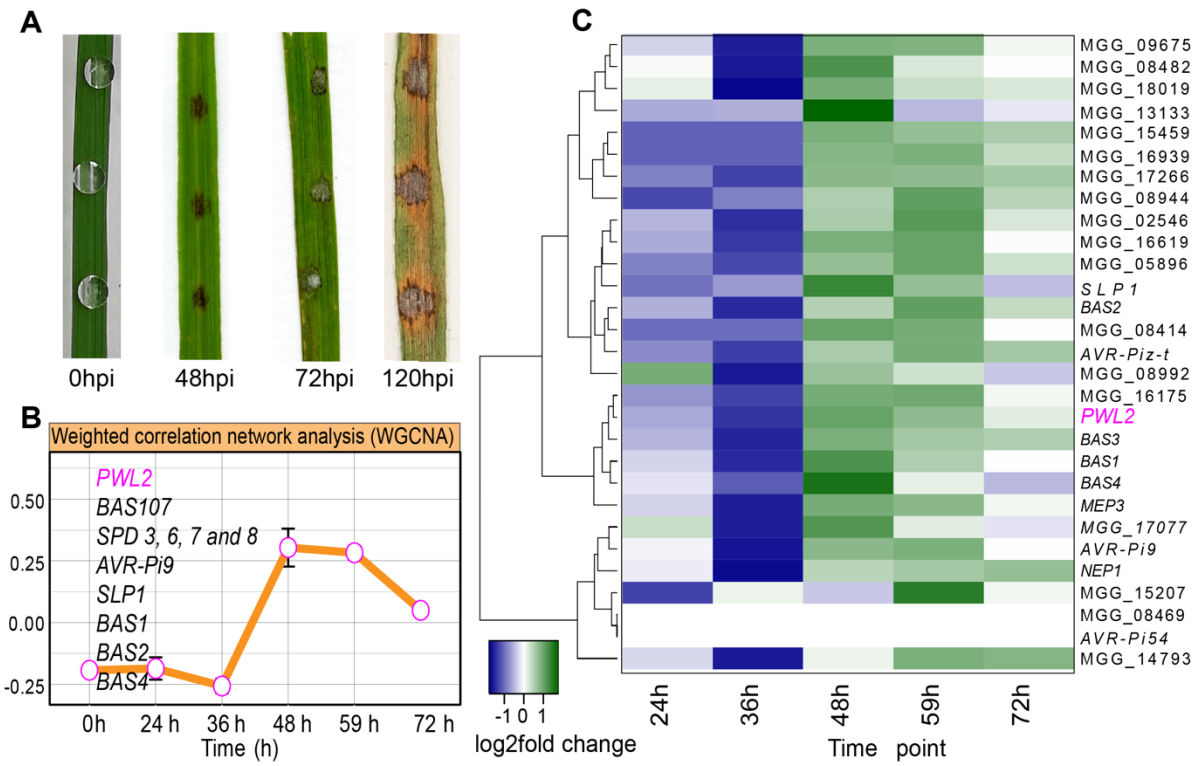

Fig. S1. *M. oryzae* Pwl2 is co-expressed during plant infection with other known effector genes.

(**A**) Attached leaves of three-weeks old rice seedlings inoculated with KE002 conidia suspension at 0, 48, 72 and 120 hpi. Samples were collected at 24, 36, 48, 59 and 72 hpi and used for RNA isolation (3 biological replicates). (**B**) RNA isolated from infected rice leaves were sequenced and the reads normalized against *M. oryzae* mycelia KE002 RNA to determine differentially expressed genes. A weighted gene co-expression network analysis grouped gene expression profile into 10 co-expression modules. The line graph (WGCNA) shows the representative eigengene for module 4 in which *PWL2* is co-expressed with other known effector protein encoding genes, *AVR-Pi9*, *SLP1*, *BAS1-4* and suppressors of cell death effectors 3, 6, 7 and 8 that possibly serve related function during biotrophic phase of invasion. (**C***)* Heatmap showing relative expression levels (log2fold change) of *PWL2* and other known effectors during infection.

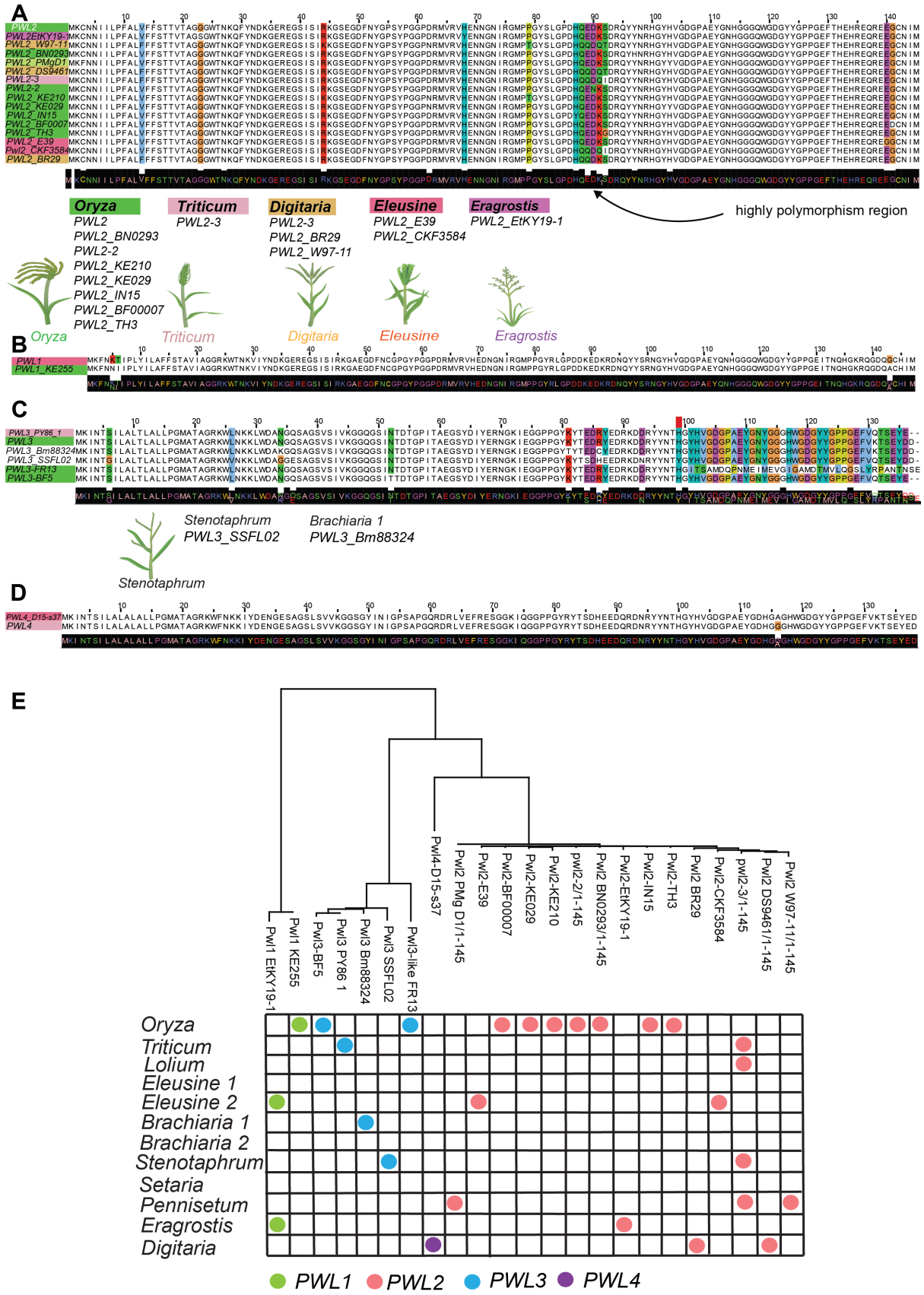

Fig. S2. *PWL2* is highly polymorphic compared to other members in the *PWL* family.

(**A**) Multiple amino acid sequence alignment of Pwl2 coding sequence and naturally occurring alleles. The region between His-87 and Ser-92 shows highest number of polymorphisms and is the region important for cognate resistance gene recognition. Multiple amino acid sequence alignment of *PWL1* (**B**), *PWL3* (**C**) and *PWL4* (**D)** Alleles identified from genomes of field isolates. Alignments were carried using ClustalW (Jalview). (**E**) Neighbor-joining tree based on amino acid sequence of alleles of the *PWL* gene family. Tree IDs contains isolate name from which allele was identified, and each dot represents presence in each host-limited form. Unlike other family members, *PWL2* alleles are present in host-limited forms apart from lineage 2 of *Brachiaria* and *Setaria. Panicum, Cynodon* and *Urochloa*-infecting isolates.

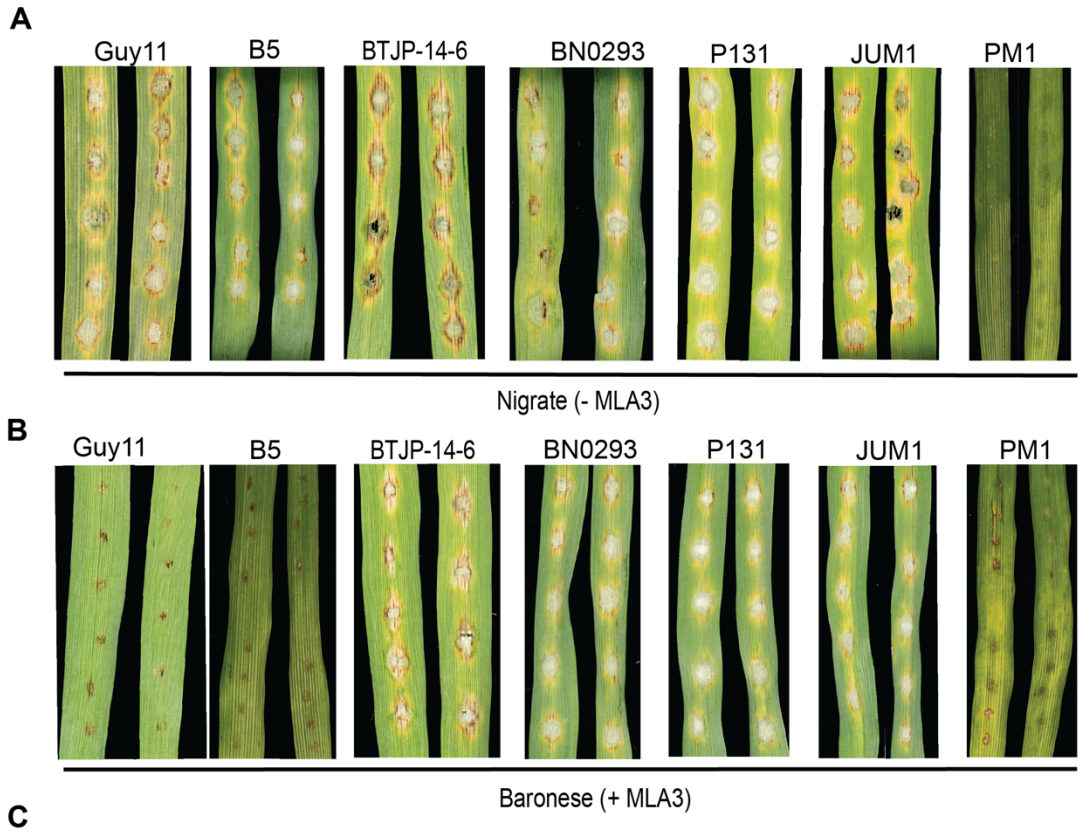

C

Isolate	Nigrate	Baronesse
Guy11	susceptible	resistant
BF5	susceptible	resistant
BTJP4-16	susceptible	susceptible
BN0293	susceptible	susceptible
P131	susceptible	susceptible
JUM1	susceptible	susceptible
PM1	resistant	resistant

Fig. S3. Two *PWL2* alleles are not recognized by the barley resistance gene Mla3.
A subset of isolates carrying alleles of *PWL2* were used in leaf drop inoculation on (**A**) barley accessions cv. Nigrate (-*Mla3*) and (**B**) cv. Baronesse (+*Mla3*). Conidial suspensions at 1 ×10^5 mL^{-1} spores/mL were harvested from Guy11 and selected isolates with *PWL2* alleles and used to inoculate 10-day-old seedlings of cv. Nigrate (-*Mla3*) and cv. Baronesse (+*Mla3*). Disease lesions were scored 5 days post-infection. Isolates BF5 (variant *Pwl2*), BTJP4-16 (*pwl2-3)*, BN0293 (variant *Pwl2*), PM1 (variant *Pwl2*), Guy11 (+*PWL2*), JUM1 (*pwl2-2*), and P131 (-*PWL2*) were used for leaf drop infection assay. As expected Guy11 could infect cv. Nigrate but not cv. Baronesse. BF5 and PM1 did not produce blast disease on barley cv. Baronesse, suggesting they express *PWL2* alleles recognised by Mla3, (or express effectors recognised by additional R-genes contained (in barley cv. Baronesse). Notably, PM1 could also not infect cv. Nigrate (-*Mla3*). P131 does not carry *PWL2* and caused blast disease on cv. Baronesse as expected. JUM1 (*pwl2-2*), BTJP4-16 (*pwl2-3)* and BN0293 (*pwl2-BN0293*) all caused blast

disease on cv. Baronesse (**C**) Summary of disease reaction of isolates with distinct *PWL2* alleles on Nigrate (-*Mla3*) and Baronesse (+*Mla3*). Observations were consistent in three independent infection replicates.

1309

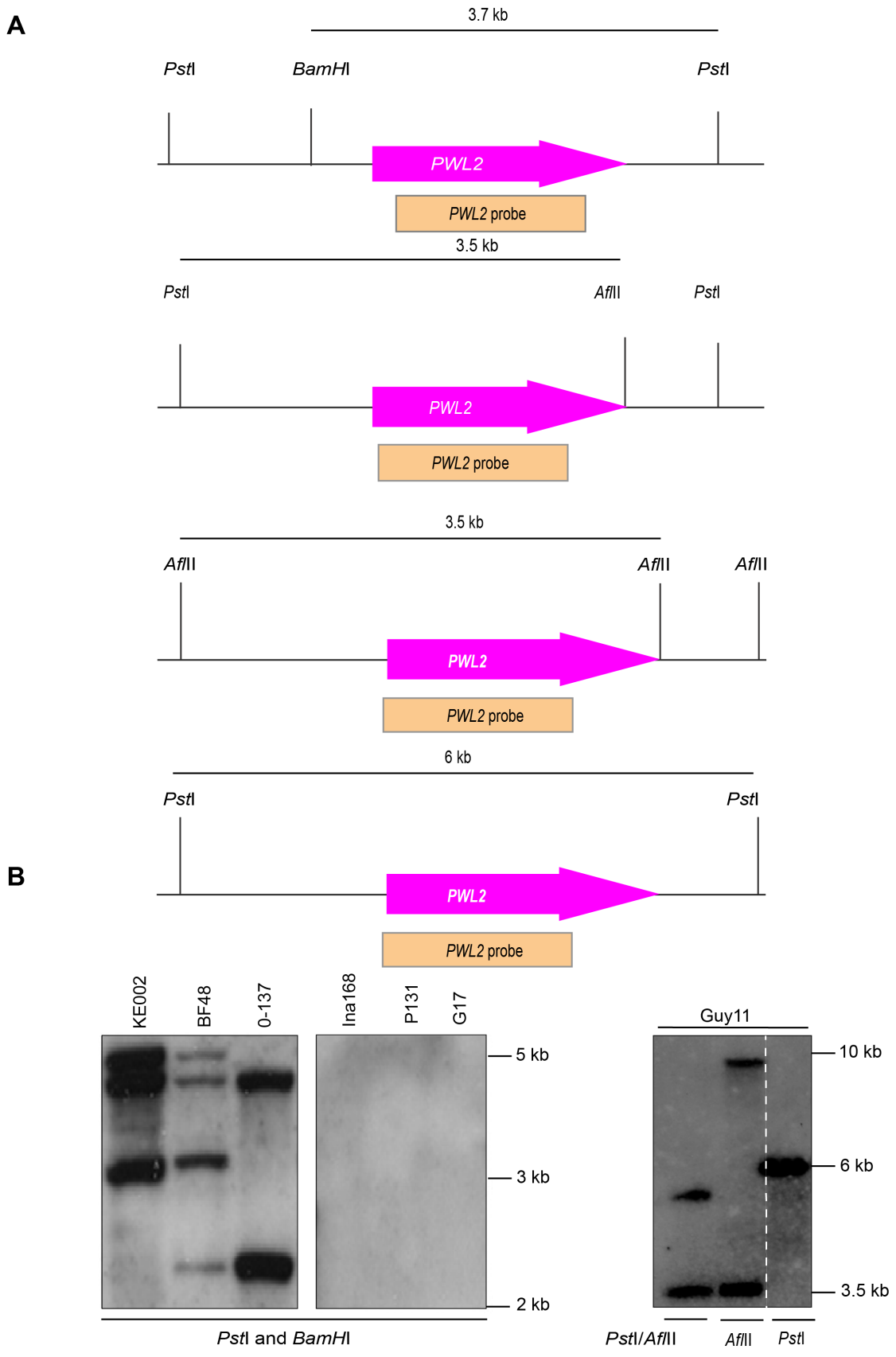
A
3.7 kb
PstI
BamHI
PstI
PWL2
PWL2 probe
3.5 kb
PstI
AflII
PstI
PWL2
PWL2 probe
3.5 kb
AflII
AflII
AflII
PWL2
PWL2 probe
6 kb
PstI
PstI
PWL2
PWL2 probe
B
KE002
BF48
0-137
Ina168
P131
G17
5 kb
3 kb
2 kb
PstI and BamHI
Guy11
10 kb
6 kb
3.5 kb
PstI/AflII
AflII
PstI

1310

1311 **Fig. S4. Southern blot analysis to determine copy number variation of *PWL2* in selected**
1312 ***M. oryzae* isolates.**
1313 (**A**) Genomic DNA was digested using different enzyme combination *Bam*HI/*Pst*I (upper
1314 panel), *Pst*I/*Afl*II (upper middle panel), *Afl*II single digest (lower middle panel) or *Pst*I single
1315 digest (lower panel) and probed using the *PWL2* 438 bp probe. Size estimates are from the
1316 *PWL2* loci annotated *M. oryzae* 70-15 genome. (**B**) Left panel, the order of digested genomic
1317 DNA from different isolates is indicated on the lanes. Right panel, when Guy11 genomic DNA
1318 was digested using *Pst*1 and *Afl*II, we detected two bands of 3.5kb and 6kb. When digested
1319 with *AflII in a* single digest were detected two bands of 3.5 kb and 10 kb. While in a single
1320 digest using *Pst*I only produce a single band of 6.5 kb.
1321
1322

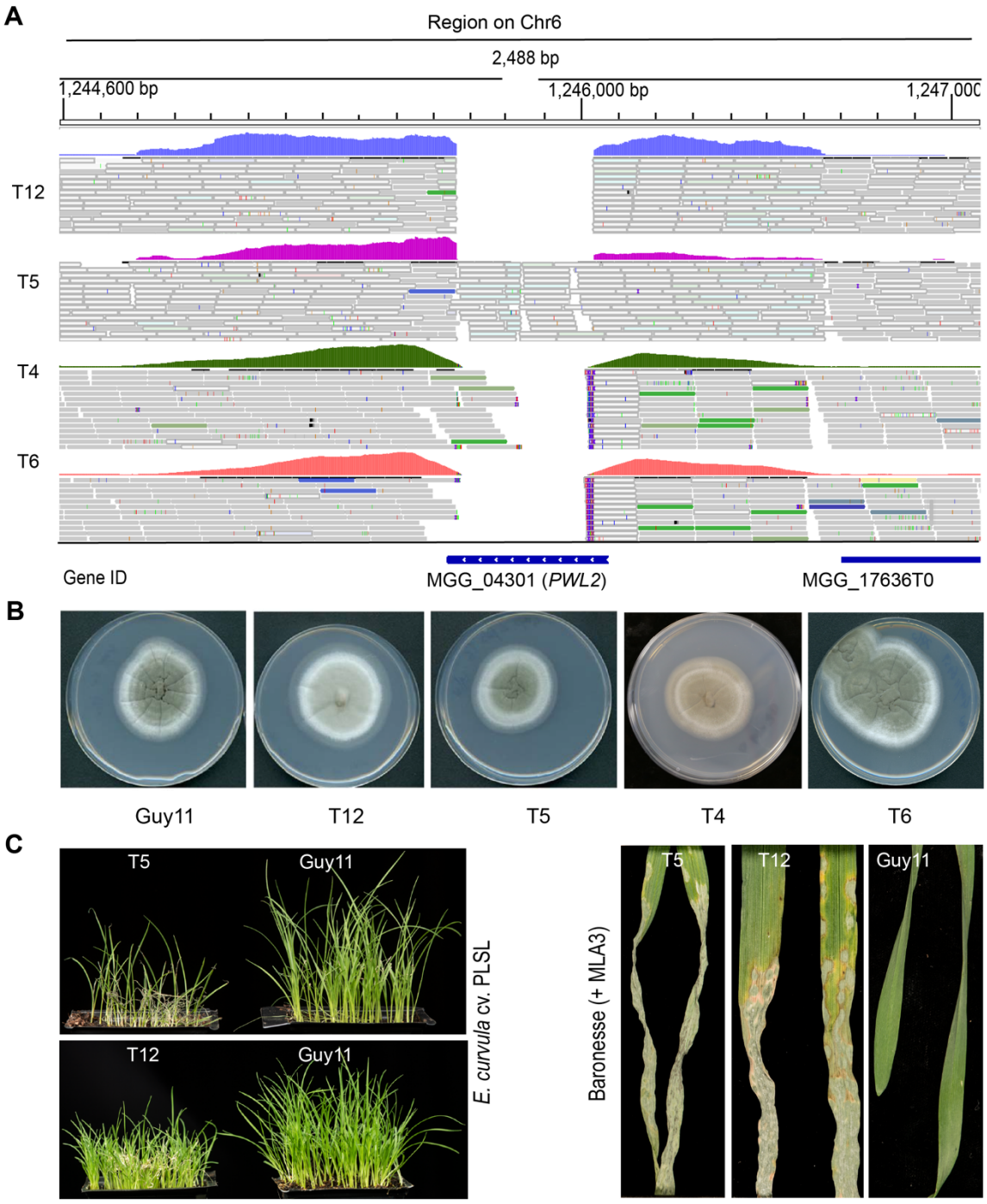

Fig. S5. *M. oryzae Δpwl2* deletion mutants show gain of virulence on weeping lovegrass and cultivar Baronesse (*Mla3*).

(**A**) Reads alignment display of *PWL2* locus on Chromosome 6 from four sequenced *pwl2* mutant strains, T12, T5, T4 and T6 (lower panel). No reads aligned to the MGG_04301T0 (*PWL2*) locus for T6 and T12 and partial alignment for T4 and T5. Read depth around *PWL2* locus is higher compared to the neighbouring gene MGG_17636T0 suggesting the *PWL2* locus occurs multiple times. Read coverage and locus length are indicated. (**B**) Guy11, T12, T5, T4,

T6 were grown at 25^0 C, on CM media for 10 days before imaging. **(C)** Disease symptoms on weeping lovegrass (*E. curvula*) and barley cultivar Baronesse (*Mla3*) to show gain of virulence for CRISPR-Cas9 deletion mutants T5 and T12. Conidial suspensions at 1×10^5 mL^{-1} spores/mL from Guy11, *Δpwl2* (T5) and *Δpwl2* (T12) were used to inoculate 10-day-old seedlings of barley cultivar Baronesse (*Mla3*) or weeping lovegrass, and disease symptoms recorded after 5 dpi. Observations were consistent in three independent infection replicates.

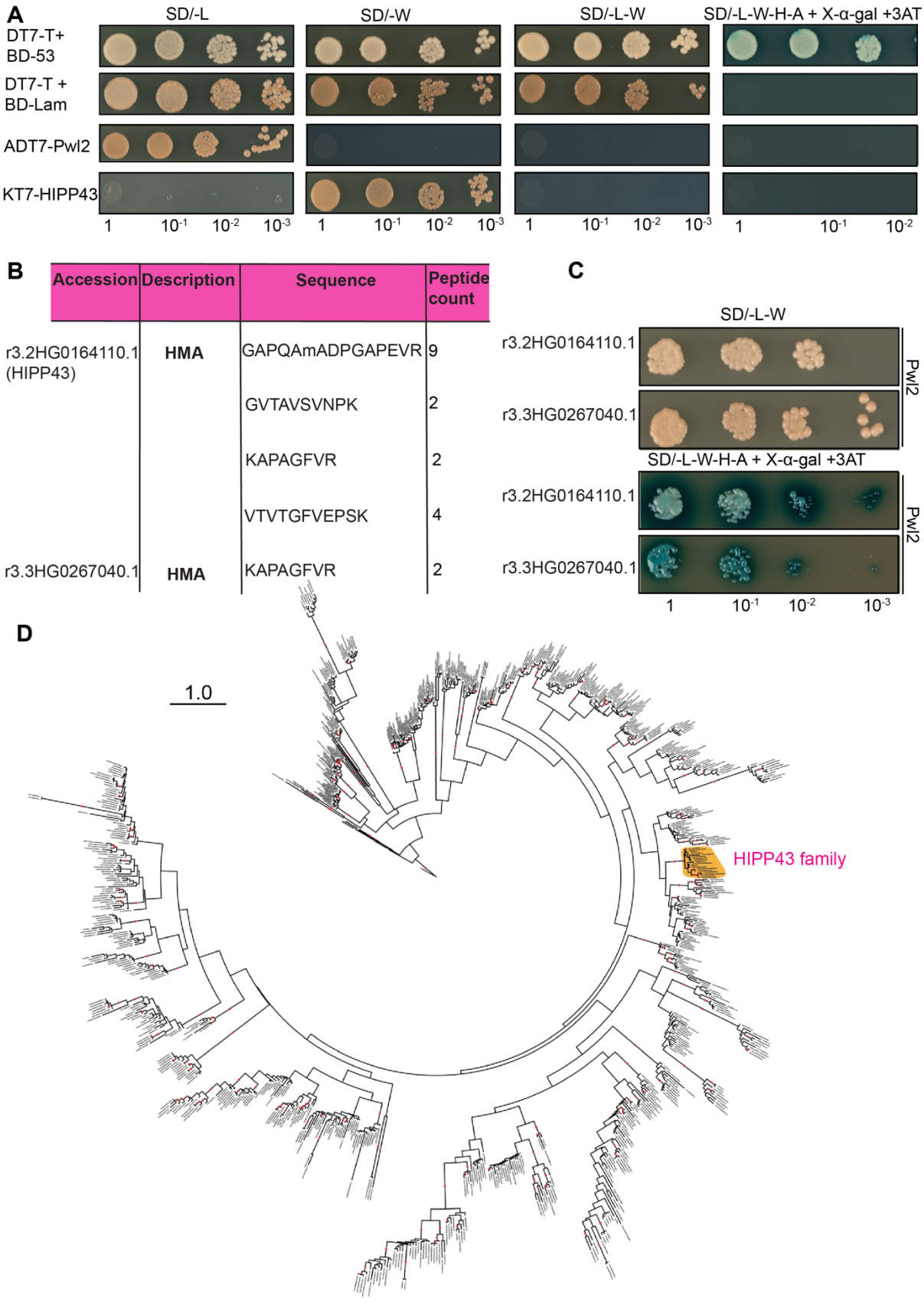

Accession	Description	Sequence	Peptide count
r3.2HG0164110.1 (HIPP43)	HMA	GAPQAmADPGAPEVR	9
		GVTAVSVNPK	2
		KAPAGFVR	2
		VTVTGFVEPSK	4
r3.3HG0267040.1	HMA	KAPAGFVR	2

Fig. S6. Pwl2 interacts with two copies of *Hv*HIPP43 identified by IP-MS.

1341 **(A)** Y2H assay to show that Pwl2 (in pGADT7 vector) and HIPP43 (in pGBKT7 vector) do
1342 not show autoactivity (**B**) Table showing peptides identified by LC-MS that mapped to two
1343 copies of HIPP43. (**C**) Pwl2 interacts with the two copies of HIPP43 in a yeast-two-hybrid
1344 assay. (**D**) Maximum likelihood phylogenetic tree of HMA domains from diverse grass species.
1345 HMA domains were identified from proteins from the grass species *B. distachyon*, *H. vulgare*,
1346 *T. aestivum*, *O. sativa*, *Oropetium thomaeum*, *Sorghum bicolor*, *Setaria italica*, and *Zea mays*.
1347 Structure guided multiple sequence alignment was performed using MAFFT-DASH and
1348 phylogenetic analysis with RAxML (v8.2.12). Scale bar indicates substitutions per site. Dots
1349 on branches indicate support of 80% or more based on 1,000 bootstraps. The HIPP43 family
1350 formed a distinct clade with bootstrap support of 98%.
1351

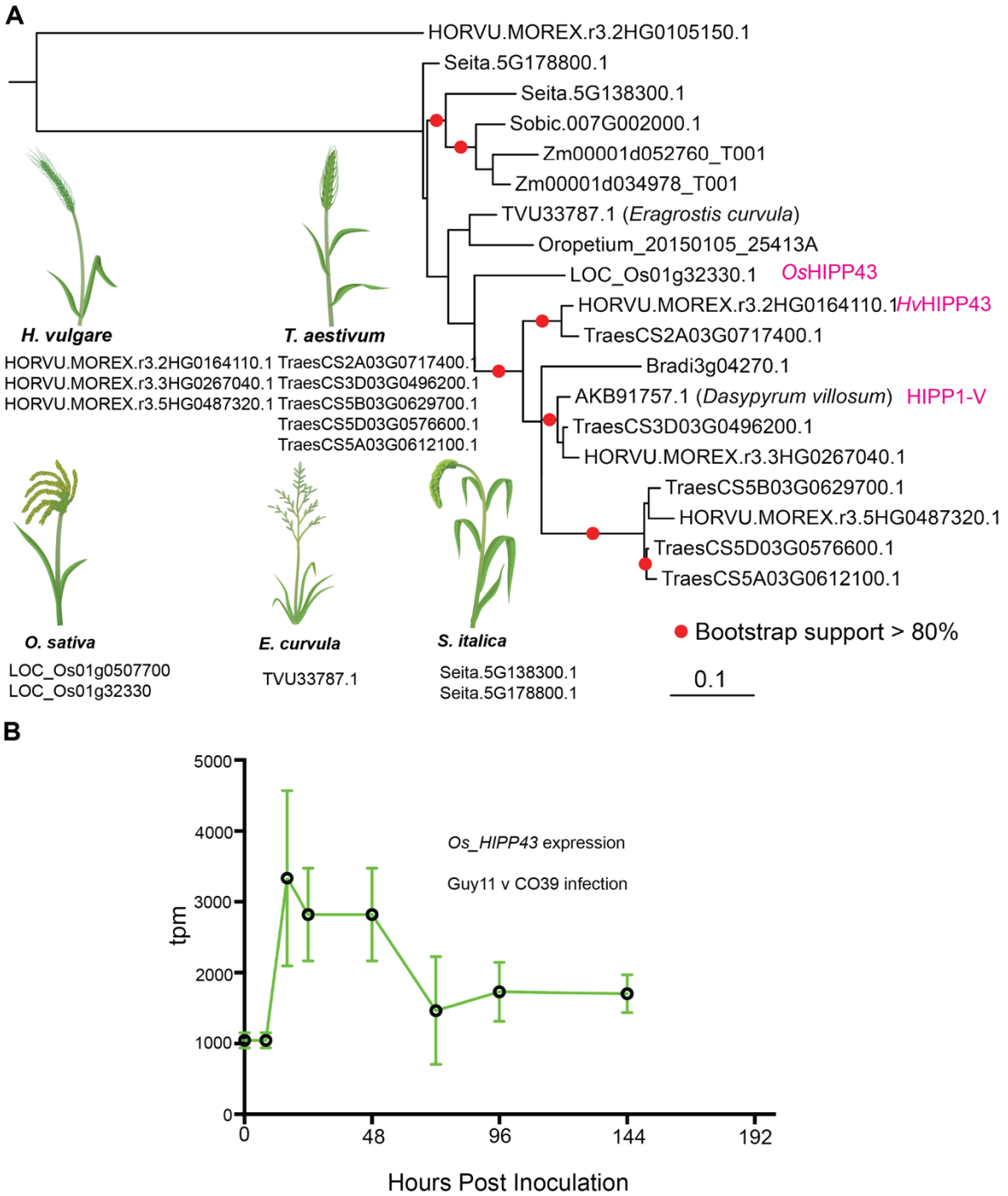

Fig. S7 Phylogenetic analysis of HIPP43 and expression profile during the rice blast infection on a susceptible rice cv. CO39.

(**A**) Full length coding sequence was identified for HIPP43 gene family members, aligned using MUSCLE translation alignment, and phylogenetic analysis with RAxML (v8.2.12). Barley and wheat (i.e. *Triticeae* lineage) have three copies of HIPP43 per haploid genome. Dots on branches indicate support of 80% or more based on 1,000 bootstraps. (**B**) RNA-seq analysis of

1359 *OsHIPP43* expression during infection of a susceptible rice cv. CO39 by Guy11. Hour post
1360 inoculation is shown on the X –axis. HIPP43 expression is shown as relative mean expression
1361 TPM (transcripts per million) at different stages of infection.
1362
1363

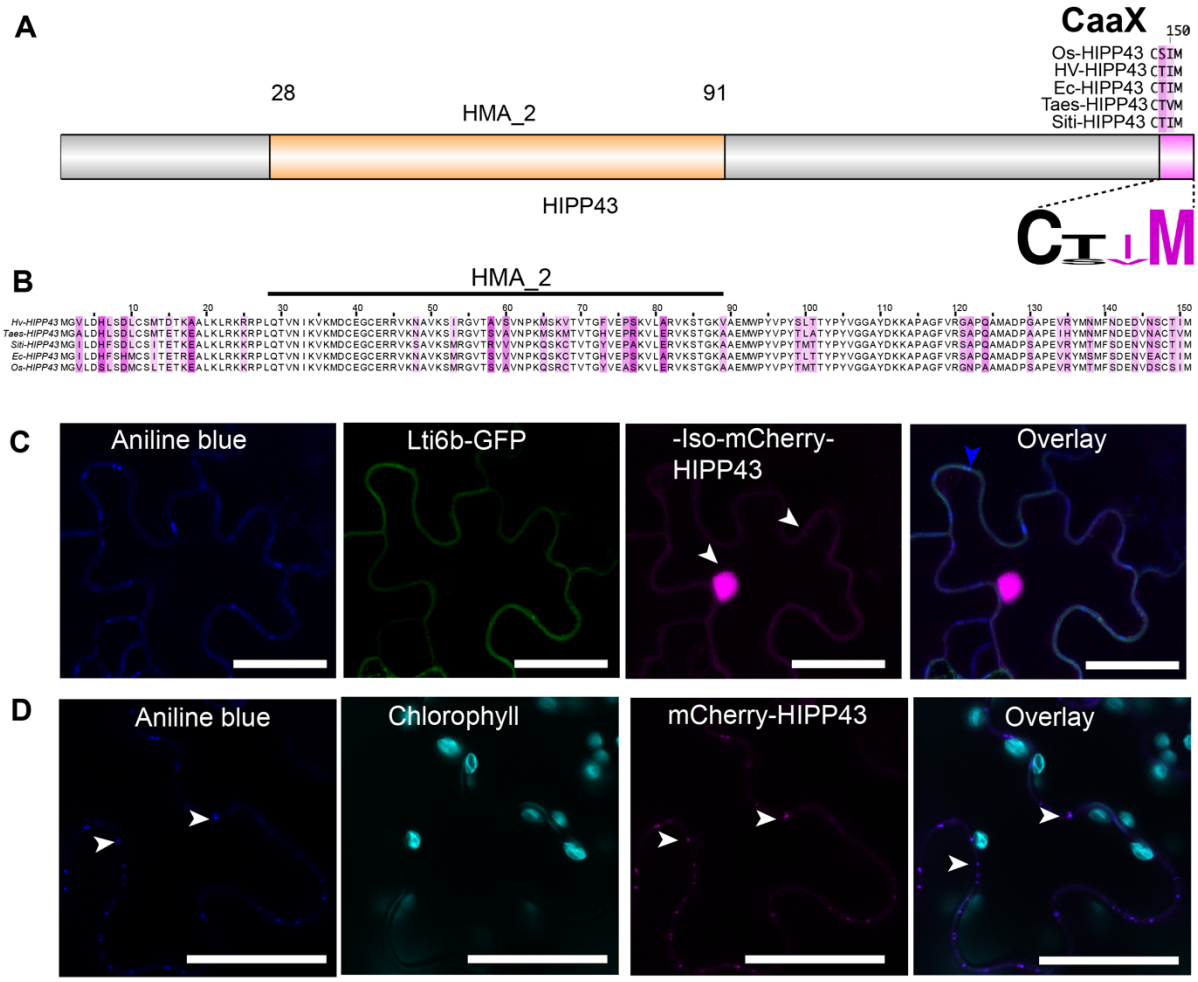

Fig. S8. HIPP43 isoprenylation motif is required for PD localisation.

(**A** +**B**) A schematic representation of domain structure of HIPP43 showing the HMA domain region and the isoprenylation motif at the C-terminus. Residues occurring at the C-terminus of HIPP43 orthologs in rice (Os-HIPP43), wheat (Taes-HIPP43), foxtail millet (Siti-HIPP43) and weeping lovegrass (Ec-HIPP43) are indicated. A multiple alignment was generated using Clustal X in Jalview and the conserved motif visualized on Weblogo. (**C-D**) Micrographs showing localization of HIPP43 without the isoprenylation motif (-Iso-mCherry-HIPP43) and of WT mCherry-HIPP43. (**C**) Deletion of the isoprenylation abolishes PD localisation but HIPP43 localises in the nucleus, the plasma membrane after 48h. Co-expression with a plasma membrane marker LTi6b-GFP and aniline blue staining confirmed localisation at the plasma membrane and lack of PD localisation. White arrows indicate regions of HIPP43 localisation away from aniline blue stained PD **(D)** Micrographs showing typical mCherry-HIPP43 localizing as small puncta on the plasma membrane when expressed in *N. benthamiana.* Staining of callose using aniline blue overlaps with mCherry-HIPP43, confirming mCherry-

1379 HIPP43 localises exclusively at PD. White arrows indicate regions of co-localisation between
1380 HIPP43, and aniline blue stained PD. Scale bars represent 20 µm.

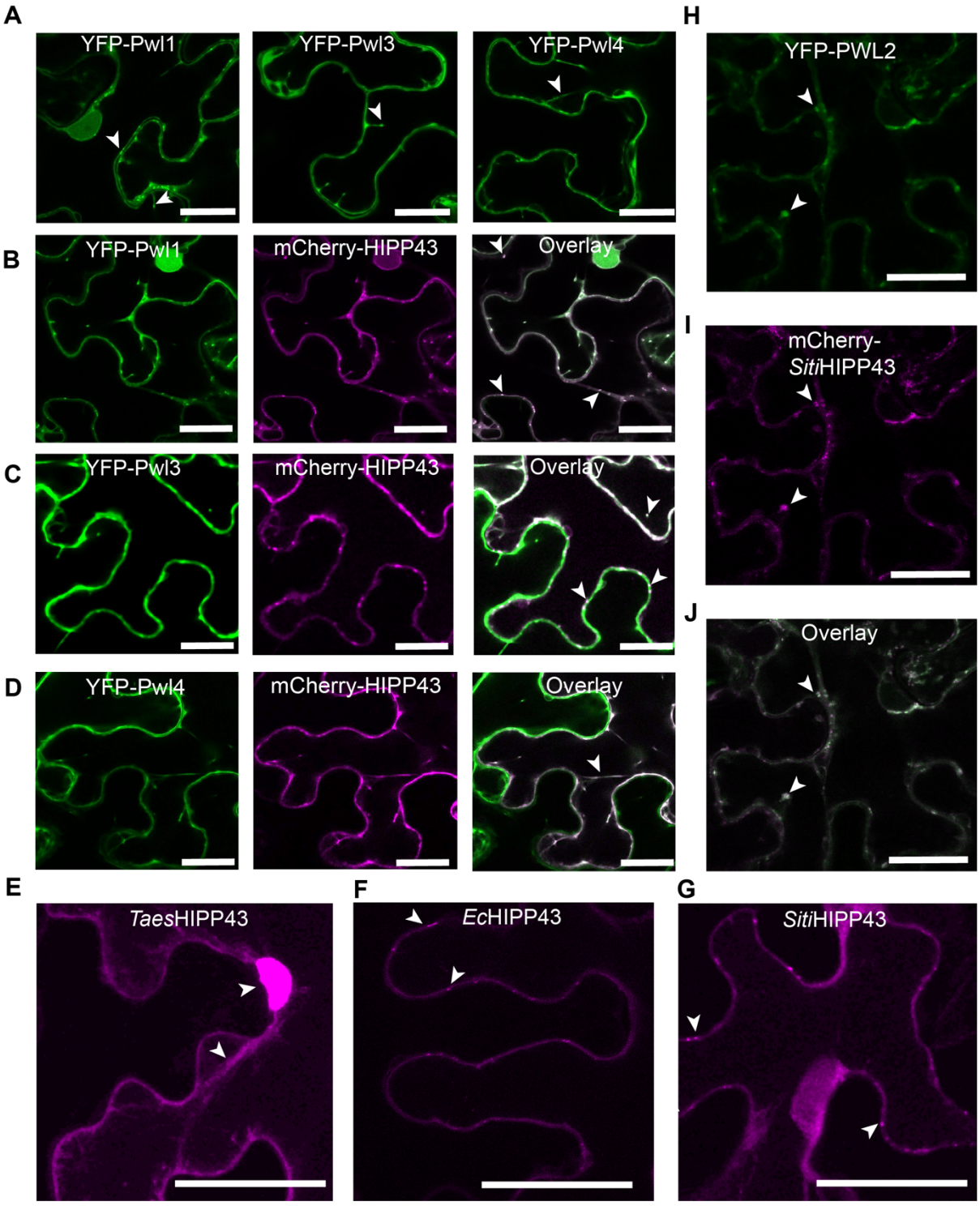

Fig. S9. Pwl1, Pwl3, Pwl4 co-localise with HIPP43 and Pwl2 co-localises with HIPP43 orthologs from other grass species.

(**A**) Micrographs showing localization of YFP-Pwl1, YFP-Pwl3 and YFP-Pwl4. Like YFP-Pwl2, Pwl1, Pwl3 and Pwl4 showed localisation in cytoplasm and cytoplasmic mobile structures. **(B-D)** Micrographs showing co-localisation of Pwl1, Pwl3 and Pwl4 with m-Cherry-HIPP43. **(B)** In presence of Pwl1 mCherry-HIPP43 translocates to the cytoplasm and

1388 partially in cytoplasmic mobile structures. **(C)** Pwl3 did not dislodge mCherry-HIPP43 from
1389 the PD while Pwl4 **(D)** only showed cytoplasmic co-localisation. (**E-G**) Micrographs showing
1390 HIPP43 orthologs fluorescently tagged to mCherry. (**E**) *Taes*HIPP43 (wheat) localizes in the
1391 nucleus and cytoplasm while (**F**) *Ec*HIPP43 (weeping lovegrass) (**G**) *Siti*HIPP43 (foxtail
1392 millet) localize as small puncta equivalent to PD. Images shown as maximum projections **(H-**
1393 **J)** Micrographs showing co-localisation of YFP-Pwl2 with mCherry-*Siti*HIPP43. mCherry-
1394 *Siti*HIPP43 localisation, was altered to the cytoplasm, cytoplasmic mobile structures. mCherry-
1395 *Siti*HIPP43 fluorescence signal was higher in presence of YFP-Pwl2. White arrows indicate
1396 regions of co-localisation and blue arrows show aniline blue stained PD. Scale bars represent
1397 20 µm.
1398
1399

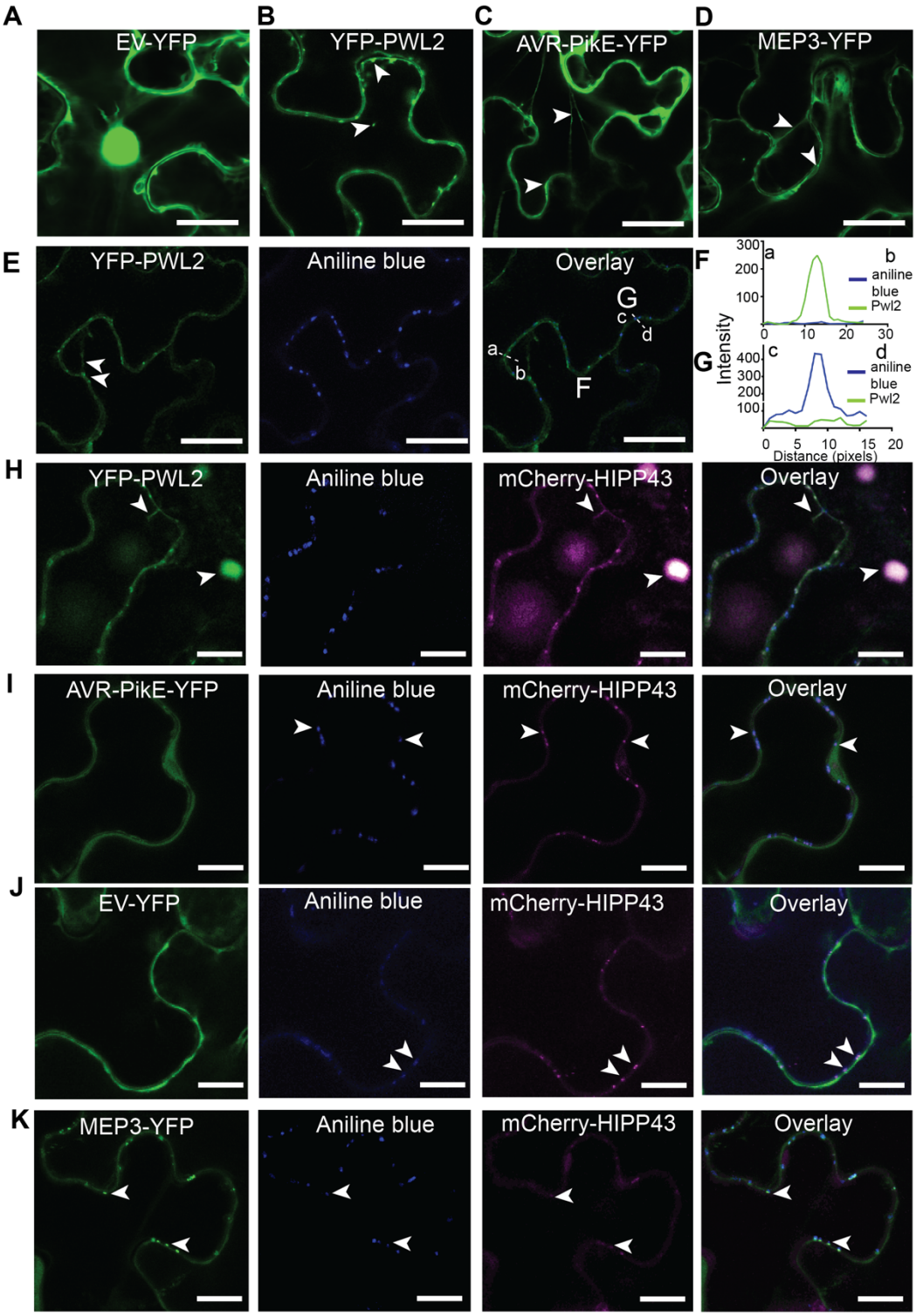

Fig. S10. Pwl2 stabilises and promotes HIPP43 cytoplasmic localisation.

(**A-D)** Micrographs showing localization of free-YFP (**A**), AVR-PikE-YFP (**B**), YFP-Pwl2 (**C**) and MEP3-YFP (**D**). Both free-YFP and AVR-PikE-YFP show localisation in the cytoplasm while YFP-Pwl2 showed localisation in cytoplasm and cytoplasmic mobile structures. MEP3 localises in the cytosol and PD **(E-I)** Micrographs and line scan graphs showing the presence

of YFP-Pwl2 in the cytosol and puncta. Lack of co-localization with aniline blue stain confirms that, without HIPP43, Pwl2 does not accumulate at PD but rather mobile puncta. (**H-K**) Micrographs showing changes of mCherry-HIPP43 localisation when co-expressed with (**H**) YFP-Pwl2, (**I**) AVR-PikE-YFP (**J**) EV-YFP and (**K**) MEP3-YFP. Staining of callose using aniline blue is used to differentiate between immobile PD and mobile cytoplasmic mCherry-HIPP43 co-localisation with YFP-Pwl2. In presence of AVR-PikE, EV and MEP3 aniline blue staining co-localises with immobile mCherry-HIPP43. Scale bars represent 20 µm.

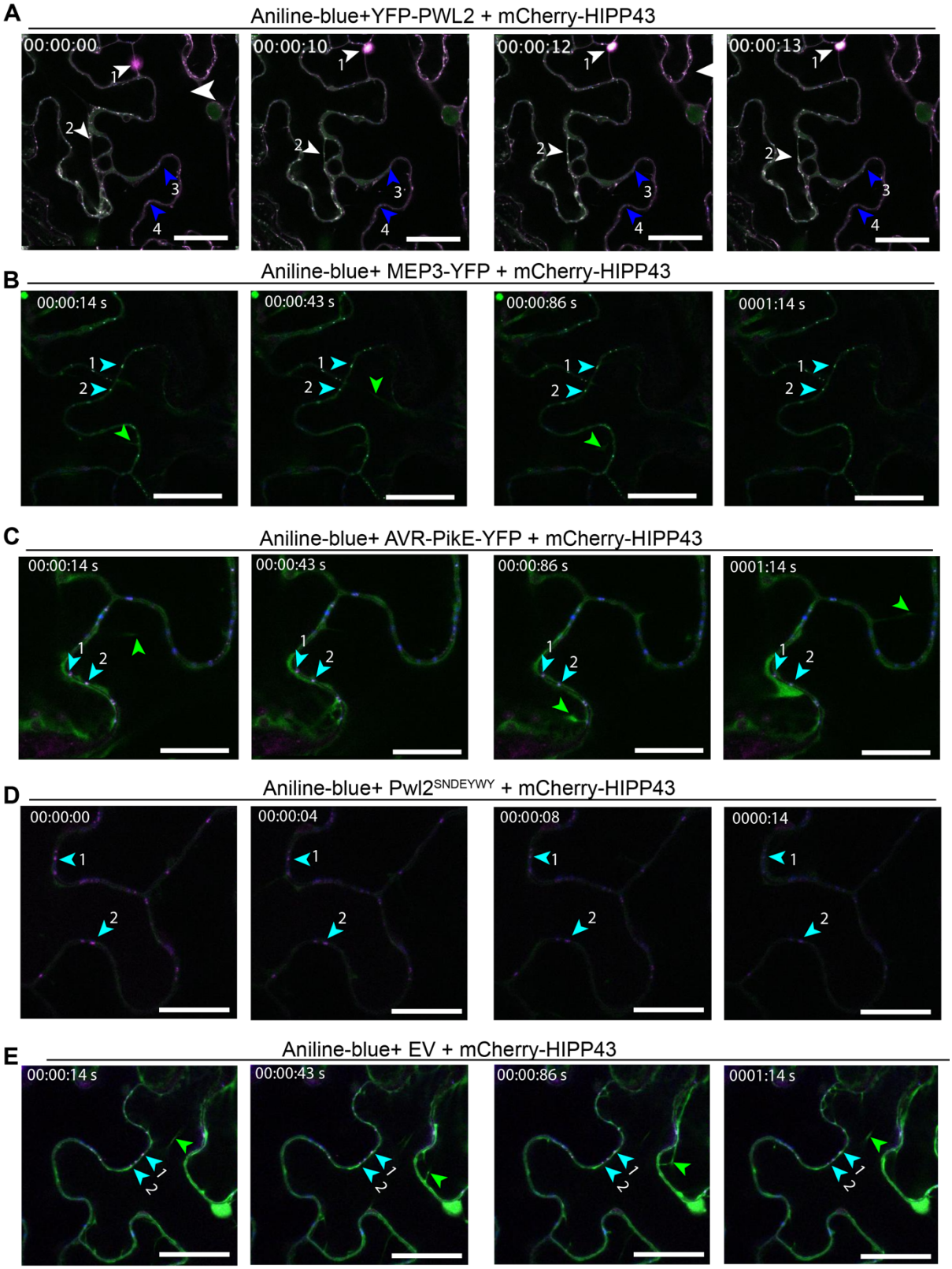

Fig. S11. Pwl2 alters HIPP43 cellular localisation from the plasmodesmata.

1422 (**A**) A time-lapse confocal microscopy micrograph to shows changes of mCherry-HIPP43
1423 localisation upon interaction with Pwl2 after co-expression in *N. benthamiana.* Pwl2 and
1424 HIPP43 co-localise as small or large mobile puncta. White arrow heads indicate mobile
1425 Pwl2/HIPP43 co-localisation puncta and blue arrow heads show immobile aniline blue stained
1426 PD. Arrow 1 indicate large cytoplasmic mobile body, arrow 2 show small mobile puncta. (**B-**
1427 **E**) Shows lack of co-localisation between MEP3 (**B**), AVR-PikE (**C**), Pwl2^{SNDEYWY} (**D**) and
1428 (**E**) free-YFP with HIPP43. HIPP43 co-localise with PD aniline blue stain as shown with cyan
1429 arrow heads and remains immobile. Note, MEP3 localises at PD in presence or absence of
1430 HIPP43. Green arrows show expression of AVR-PikE, MEP3 and free-YFP in the cytosol
1431 without HIPP43 co-localisation. Scale bars represent 20 µm. Aniline blue is shown in blue,
1432 free-YFP, Pwl2, MEP3, AVR-PikE and Pwl2^{SNDEYWY} are shown as green while mCherry-
1433 HIPP43 is shown as magenta.
1434

1435 **List of Movies**

1436 **Movie S1**

1437 Mobility of Pwl2/HIPP43 sub-cellular co-localisation cytosolic puncta, 48 h after co-
1438 expression in *N. benthamiana* cells and visualized using laser confocal microscopy. PD are
1439 visualized as callose stained with aniline blue, Pwl2 as green and HIPP43 magenta fluorescence
1440 respectively. Arrows are used to track Pwl2/HIPP43 co-localised mobile cytosolic puncta.

1441 **Movie S2**

1442 A laser confocal microscopy time-lapse video to show lack of co-localisation between AVR-
1443 PikE and HIPP43, 48 h after co-expression in *N. benthamiana* cells. PD are visualized as
1444 callose stained with aniline blue, AVR-PikE as green and HIPP43 magenta fluorescence
1445 respectively. Cyan arrows show co-localisation of aniline blue stain and HIPP43 as immobile
1446 signal at PD. Most of AVR-PikE expression occurred in the cytosol without HIPP43 co-
1447 localisation.

1448 **Movie S3**

1449 A laser confocal microscopy time-lapse video to show lack of co-localisation between MEP3
1450 and HIPP43, 48 h after co-expression in *N. benthamiana* cells. PD are visualized as callose
1451 stained with aniline blue, MEP3 as green and HIPP43 magenta fluorescence respectively. Cyan
1452 arrows show co-localisation of aniline blue stain, MEP3 and HIPP43 as immobile signal at PD.
1453 Most of MEP3 expression occurred in the cytosol without HIPP43 co-localisation.

1454 **Movie S4**

1455 A laser confocal microscopy time-lapse video to show lack of co-localisation between a
1456 septuple mutant of Pwl2, Pwl2^{SNDEYWY} and HIPP43, 48 h after co-expression in *N.*
1457 *benthamiana* cells. PD are visualized as callose stained with aniline blue, Pwl2^{SNDEYWY} as
1458 green and HIPP43 magenta fluorescence respectively. Cyan arrows show co-localisation of
1459 aniline blue stain and HIPP43 as immobile signal at PD while expression of Pwl2^{SNDEYWY}
1460 remained in the cytosol without HIPP43 co-localisation

1461 **Movie S5**

1462 A laser confocal microscopy time-lapse video to show lack of co-localisation between free-
1463 YFP and HIPP43, 48 h after co-expression in *N. benthamiana* cells. laser confocal microscopy.
1464 PD are visualized as callose stained with aniline blue, free-YFP as green and HIPP43 magenta
1465 fluorescence respectively. Cyan arrows show co-localisation of aniline blue stain and HIPP43
1466 as immobile signal at PD while expression of free-YFP remained in the cytosol without HIPP43
1467 co-localisation.

1468 **Table S1 Primers used in this study.**

1469 **Supplemental Data 1. Blast genomes used for phylogenetic analysis.**

1470 **Supplemental Data 2. Blast genomes used for copy number variation analysis.**

1471 **Supplemental Data 3. IP-MS spectrum report.**

1472 **Supplemental Data 4. IP-MS samples report with clusters.**

1473

1474

1475

1476 **Table S1 Primers used in this study.**

1477

Primer	Sequence
PWL2ORF	ATGAAATGCAACAACATCATCCTCCC
PWL2ORR	ACATAATATTGCAGCCCTCTTCTCGC
PWL2f	GGTTCTTATTATGGTCCCGGGTGA
PWL2r	GGTTCTTATTATGGTCCCGGGTGA
PWL2848F	CGCGGTGGCGGCCGCTCTAGAGACCGGGCACGAACCCGG CAGGC
PWL2-R	CATAATATTGCAGCCCTCTT
PWL2_GFPF	GGGCTGCAATATTATGATGGTGAGCAAGGGCGAGGAGCT G
KOLFF	ACAACGCGGTGTAAAGATTCGGGT
KOLFR	GTCGTGACTGGGAAAACCCTGGCGAGACCAAAGCAAAAG GGAGGATGA
KORFF	TCCTGTGTGAAATTGTTATCCGCTGCGAGAAGAGGGCTGC AATATTA
PG514-myc-F	AACACGGGGGACTCTAGAGAACAAAAGTTGATCTCTGA
YFPPWL2-F	GACGAGCTGTACAAGGGTGGCGGGTGGACTAAC
PWL2-N-term-YFPR	GTTAGTCCACCCGCCACCCTTGTACAGCTCGTC
PWL2-R-p514	GAACGATCGGGGAAATTCGTTACATAATATTGCAGCCCT
HAPwl2F	AGAGAACACGGGGGACTCTAGAATGGGTGGCGGGTGGAC TAAC
PG514-myc-F	AACACGGGGGACTCTAGAGAACAAAAGTTGATCTCTGA
myc-HIPP43-R	TCCAAGACGCCCATAAGGTCCTCTTCAGAAA
myc-HIPP43F	ATTTCTGAAGAGGACCTTATGGGCGTCTTGGA
HIPP43-NOS-R	ACGATCGGGGAAATTCGTCACATGATGGTGCAG
PG514-mCherry-F	AACACGGGGGACTCTAGAATGGTGAGCAAGGGC
mCherry-HIPP43F	GGACGAGCTGTACAAGATGGGCGTCTTGGA
mCherry-HIPP43R	TCCAAGACGCCCATCTTGTACAGCTCGTCC
KT7_HIPP34F	CATGGAGGCCGAATTCATGGGCGTCTTGGA
KT7_HIPP34R	GCAGGTCGACGGATCCTCACATGATGGTGCAG

1478